Journal of Molecular Modeling (2023) 29:204
https://doi.org/10.1007/s00894-023-05596-3

ORIGINAL PAPER

A computational and laboratory approach for the investigation of interactions of peptide conjugated natural terpenes with EpHA2 receptor

Beatriz G. Goncalves[1] · **Ipsita A. Banerjee**[1]

Received: 6 July 2022 / Accepted: 17 May 2023 / Published online: 8 June 2023

Abstract

Context Ephrin type A receptor 2 (EphA2) is a well-known drug target for cancer treatment due to its overexpression in numerous types of cancers. Thus, it is crucial to determine the binding interactions of this receptor with both the ligand-binding domain (LBD) and the kinase-binding domain (KBD) through a targeted approach in order to modulate its activity. In this work, natural terpenes with inherent anticancer properties were conjugated with short peptides YSAYP and SWLAY that are known to bind to the LBD of EphA2 receptor. We examined the binding interactions of six terpenes (maslinic acid, levopimaric acid, quinopimaric acid, oleanolic, polyalthic, and hydroxybetulinic acid) conjugated to the above peptides with the ligand-binding domain (LBD) of EphA2 receptor computationally. Additionally, following the "target-hopping approach," we also examined the interactions of the conjugates with the KBD. Our results indicated that most of the conjugates showed higher binding interactions with the EphA2 kinase domain compared to LBD. Furthermore, the binding affinities of the terpenes increased upon conjugating the peptides with the terpenes. In order to further investigate the specificity toward EphA2 kinase domain, we also examined the binding interactions of the terpenes conjugated to VPWXE (x = norleucine), as VPWXE has been shown to bind to other RTKs. Our results indicated that the terpenes conjugated to SWLAY in particular showed high efficacy toward binding to the KBD. We also designed conjugates where in the peptide portion and the terpenes were separated by a butyl (C4) group linker to examine if the binding interactions could be enhanced. Docking studies showed that the conjugates with linkers had enhanced binding with the LBD compared to those without linkers, though binding remained slightly higher without linkers toward the KBD. As a proof of concept, maslinate and oleanolate conjugates of each of the peptides were then tested with F98 tumor cells which are known to overexpress EphA2 receptor. Results indicated that the oleanolate-amido-SWLAY conjugates were efficacious in reducing the cell proliferation of the tumor cells and may be potentially developed and further studied for targeting tumor cells overexpressing the EphA2 receptor. To test if these conjugates could bind to the receptor and potentially function as kinase inhibitors, we conducted SPR analysis and ADP-Glo assay. Our results indicated that OA conjugate with SWLAY showed the highest inhibition.

Methods Docking studies were carried out using AutoDock Vina, v.1.2.0; Molecular Dynamics and MMGBSA calculations were carried out through Schrodinger Software DESMOND.

Keywords Terpenes · Molecular dynamics · Peptide conjugates · Tumor targeting

Introduction

Over the years, naturally occurring resources from plants have been known for their therapeutic and medicinal properties [1]. For example, essential oils such as gingerol, eugenol, and peppermint oil are plant-based compounds that have found numerous therapeutic applications due to their antioxidant, anti-inflammatory, and anticancer properties [2]. Often the active components of plant-based materials include polyphenols, flavonoids, glycosides, and several alkaloids [3, 4]. Additionally, phytochemicals including terpenoids and phytosterols have been found to possess potent anticancer activity [5]. These include terpenoids such as β-elemene, furanodiene, curcumol, and phytosterols like 24-epibrassinolide, stigamsterol [6, 7]. Many chemotherapeutics such as Paclitaxel, Vinblastine, and Camptothecin

✉ Ipsita A. Banerjee
banerjee@fordham.edu

[1] Department of Chemistry, Fordham University, 441 East Fordham Road, Bronx, NY 10458, USA

have also been derived from plants [8, 9]. Thus, research toward the development of natural product-based therapeutics is gaining importance due their relatively lower toxicity and enhanced cytocompatibility and targeting ability. In the realm of targeting, several peptide sequences with therapeutic value have also been obtained from plants, marine resources, and microbes and are known to have targeting ability toward tumor cells [10, 11]. Targeting tumor cells is significant because it not only enhances the potency of a drug, but also mitigates side effects. Thus, several tumor-targeting peptides have been developed. For example, the cyclic peptide containing the sequence CTVALPGGYVRVC was shown to preferentially internalize into melanoma tumor cells through the GRP78 receptor. [12]. In another study, the sequence TYPE7 comprising residues of the transmembrane region of the tyrosine kinase receptor EphA2, overexpressed in several types of cancer cells, was found to bind to the receptor and prevent cell migration [13]. In particular, the EphA2 kinase has been known to be highly implicated in carcinogenesis among the Eph kinases [14]. It is overexpressed in several types of cancers and stimulates proliferation, angiogenesis, invasion, and metastasis resulting in poor prognosis [15, 16]. It is therefore considered a promising target for cancer therapeutics. The precise role of Eph A2 kinase in tumor progression however has been a subject of debate. This is because several studies have also shown that the activation of EphA2 kinase on tumor cells can elicit signaling pathways that may also lead to tumor suppression. In fact, studies have shown that ligand stimulation of EphA2 can inhibit integrin signaling, Ras/ERK pathway, Rac GTPase activation, as well as suppress the PI3K/Akt oncogenic signaling pathways [17, 18] which in turn results in reduced cell proliferation and migration. Furthermore, it has been shown that while the regulation of cell migration, adhesion, invasion, and metastasis is affected by the kinase-dependent role of EphA2 receptor, invasion and metastasis may also occur in an EphA2 kinase-independent way [19]. Under those circumstances, the reactivation of the EphA2 kinase function becomes necessary. Therefore, further studies are necessary to develop and examine interactions of novel drug candidates with the EphA2 kinase domain.

The EphA2 receptor belongs to the Eph family of RTKs that comprises of an extracellular ligand-binding domain (LBD), a cysteine-rich domain, an epidermal growth factor (EGF)-like domain and two fibronectin type III domains. The juxtamembrane region and tyrosine kinase domain, as well as the sterile α motif (SAM) and the C-terminal PDZ-binding motif, are part of the intracellular region [20]. Ephrin A1 is the primary ligand that binds to EphA2 receptor resulting in the formation of signal-receptor complex. Researchers have developed peptide agonists such as YSAYPDSVPMMS and SWLAYPGAVSYR that can mimic Ephrin ligands. In particular, YSAYPDSVPMMS binding promotes forward signaling, resulting in EphA2 phosphorylation and internalization [21] and is considered as a potential tumor-homing peptide that can be utilized for drug delivery to tumor cells. To that end, nanoscale materials functionalized with YSAYPDSVPMMS have been developed, and were found to target overexpressed EphA2 receptors in ovarian tumor cells [22, 23]. It has also been reported that YSAYPDSVPMMS enhances EphA2 stability, by promoting EphA2 dimer stabilization, which leads to enhanced kinase activity and reduced cell migration [24]. In a recent study, the crystal structure of the unphosphorylated intracellular region of the EphA2 receptor was solved by Pasquale and co-workers [25]. Interestingly, the mechanism of EphA2 overexpression related tumorigenesis is markedly different from that of other RTKs such as EGFR where in tumorigenesis is promoted due to uncontrolled dimerization that leads to further downstream signaling [26]. Therefore, inhibitors of receptor kinase activity similar to those that are currently being developed for other RTKs may work differently for EphA2. Thus, it is important to examine the binding interactions of newly developed therapeutics with both the kinase and the ligand-binding domains of the EphA2 receptor and compare those with other RTKs.

In this study, we have selected six plant-based terpenes with known anti-tumor activity and conjugated those with the peptides YSAYP and SWLAY to form novel peptide conjugates for targeting the EphA2 receptor. We chose these 5-mer sequences because in previous work, it has been shown that those sequences retain selectivity toward the EphA2 receptor [27]. The terpenes include quinopimaric acid (QA), polyalthic acid (PA), levopimaric acid (LA), hydroxybetulinic acid (HB), oleanolic acid (OA), and maslinic acid (MA). In a recent study, Tognolini and co-workers utilized known ligands such as betulinic acid and OA, that are known to bind to the nuclear receptor FXR and the G-protein coupled receptor TGR5 to examine their ability to inhibit EphA2 receptor by targeting the EphA2-ephrin-A1interaction by target-hopping approach [28]. They examined the structural similarities between lithocholic acid and triterpenes such as betulinic acid, OA, as well as stilbene carboxylic acids and investigated their efficacy to inhibit Ephrin A1 interaction with EphA2 receptor. Lithocholic acid, which contains a steroidal moiety, was used as the starting point as it has been known to display antagonistic activity for EphA2 receptor and has significant structural similarities with the terpenes. Furthermore, mechanistically, it has been shown that lithocholic acid interferes with EphA2-ephrin ligand interaction through EphA2-kinase activation [29]. Although they reported that the stilbene carboxylic acid compounds had the highest ability to interrupt EphrinA1-EphA2 receptor interaction, both OA and betulinic acid also showed modest ability to disrupt this interaction. We therefore hypothesized, that given that these

triterpenes are precursors of steroids [30] and have structural similarities, the binding interactions with EphA2 receptor may be further enhanced by conjugating a range of terpenes with short peptide sequences that are known to specifically bind to EphA2 receptor. In fact, it was shown that lithocholic acid when conjugated to amino acids such as tryptophan and phenylalanine showed high antagonistic activity toward the receptor [31]. While previous work mainly focused on the ligand-binding domain interactions, we have extended it to the kinase binding domain as some of the terpenes utilized in this study have been known to react with other types of kinases. For example, in previous work, it has been shown that terpenes such as MA have been found to inhibit the activity of kinases such as PKC in lymphoblastoid cells [32]. Additionally, its involvement in mTORC1 activation was recently proven [33]. OA is another anticancer compound that has also been found to bind to cyclin-dependent kinases and cause inhibition of tumor cell proliferation [34]. Other terpenes such as PA have also been tested for kinase binding. Given these studies, we conjectured that by utilizing the "target hopping approach" and conjugating these terpenes with anticancer properties to the short peptides YSAYP and SWLAY may also result in kinase binding of the EphA2 receptor kinase domain and interact with the binding pocket of the receptor. These terpenes or their derivatives have been shown to possess anti-inflammatory, anti-microbial, anti-viral, anti-tumor, and anti-ulcerative activity and are therefore attractive molecules for drug design [35–38]. To examine conjugate targeting, we explored their binding interactions with both the kinase- and ligand-binding domains. Furthermore, we also conjugated the terpenes with an EGFR-targeting peptide VPWXE (where X represents norleucine) [39] and explored the binding interactions of VPWXE-conjugated terpenes with EphA2 ligand-binding domain (LBD) and EphA2 kinase domain (KBD) to examine specificity of binding. We also studied the interactions of the control peptides and the unconjugated terpenes using molecular docking and molecular dynamics studies. The chemical structures of the designed peptide conjugates are shown in Fig. 1. To further evaluate if a linker could enhance binding interactions, we also designed conjugates and carried out in silico studies where in the carboxylic acid groups of the terpenes were conjugated to the free amino group of 5-amino valeric acid (creating a C4 hydrophobic linker) which was then further conjugated with the amino terminal of the 5-mer peptides. Those structures are shown in Supplementary Information Fig. S1.

Finally, as a proof of concept, we synthesized conjugates of the terpenes MA and OA with all three of the peptides and examined their potency to target F98 tumor cells that are known to overexpress EphA2 receptor. Our results indicated that OA-conjugates of the peptides, particularly with SWLAY, showed lowered proliferation of tumor cells. Additionally, no effect was seen in non-tumor cells (fibroblasts). Furthermore, ADP-Glo assay results revealed that the OA-amido-SWLAY conjugates showed the highest kinase inhibition, while the VPWXE conjugates showed minimal inhibition. Surface plasmon resonance (SPR) analysis also confirmed that oleanolate-amido-SWLAY conjugates bound to the kinase-binding domain with higher affinity. Thus, overall, OA conjugates of these peptides, particularly with SWLAY may be developed for future studies in cancer therapeutics.

Materials and methods

Materials

Maslinic acid and oleanolic acid were purchased from Santa Cruz Biotechnology. The peptide sequences, YSAYP, SWLAY, and VPW(Nle)E were custom ordered from Genscript. Dimethylformamide (DMF), *N*-hydroxysuccinimide (NHS), streptavidin, 1-ethyl-3-(3-dimethylaminopropyl) carbodiimide (EDAC), and Poly (Glu, Tyr) sodium salt were purchased from Sigma-Aldrich. Rat F98 glioma cell line (CRL-2397), and mouse fibroblast cells (SCRC-1008) were purchased from ATCC (Manassas, VA, USA) along with fetal bovine serum (FBS), Dulbecco's modified Eagle's medium (DMEM), Roswell Park Memorial Institute (RPMI) medium, and Dulbecco's phosphate-buffered saline (PBS). The WST-8 Cell Proliferation Assay Kit and the Annexin V FTIC-Propidium Iodide Assay Kit were purchased from Cayman Chemical Company (Ann Arbor, MI, USA). The ADP-Glo Kinase Assay was purchased from Promega (Madison, WI). Ephrin A2/EFNA2 Protein, Mouse, Recombinant was purchased from Sino Biological.

Methods

Structure design

The peptides YSAYP and SWLAY; terpenes QA, PA, LA, HB, OA, and MA; and their conjugates with and without linker (5-amino-valeric acid) were designed using ChemDraw (20.1.1) and then transferred to ChemDraw3D (20.1.1) for energy minimization to obtain the most stable conformation. Each structure was then saved as a.pdb file to check for structural errors in PyMOL (2.5.2) [40].

Sigma profiles and surfaces

To determine the physicochemical properties of each terpene, peptide, and conjugate, σ profiles were generated. Each chemical structure was first converted to a.sdf file on PyMOL and copied into Turbomole for ab initio quantum chemical calculations [41]. Then COSMO (conductor-like Screening model)

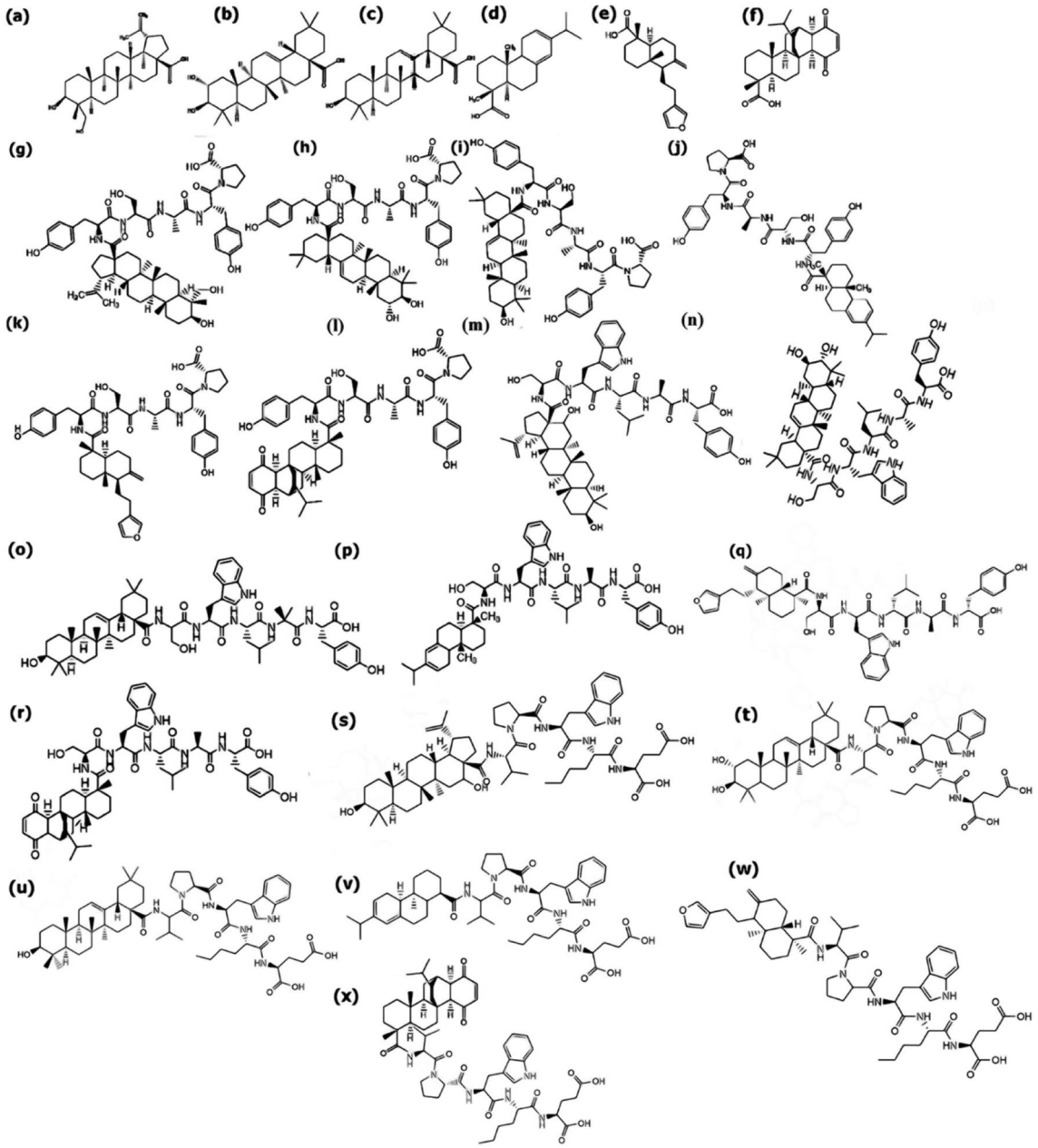

Fig. 1 Chemical structures of terpenes and their peptide conjugates. **a** Hydroxybetulinic acid (HBA); **b** MA acid (MA); **c** oleanolic acid (OA); **d** levopimaric acid (LA); **e** polyalthic acid (PA); **f** quinopimaric acid (QA); **g** HBA-YSAYP; **h** MA-YSAYP; **i** OA-YSAYAP; **j** LA-YSAYP; **k** PA-YSAYP; **l** QA-YSAYP; **m** HBA-SWLAY; **n** MA-SWLAY; **o** OA-SWLAY; **p** LA-SWLAY; **q** PA-SWLAY; **r** QA-SWLAY; **s** HBA- VPWXE; **t** MA-VPWXE; **u** OA-VPWXE; **v** LA-VPWXE; **w**PA-VPWXE; **x** QA-VPWXE. [X = norleucyl group]

calculations were generated by computing the screening charges of the surface of the molecules, similar to the dielectric continuum solvation models. A cosmo file was then input into the graphical user interface COSMOtherm (2020) [42]. COSMOtherm generated an σ profile detailing the probability distribution of specific charge densities from −0.03 to 0.03 that a molecular surface segment contains, with $\sigma < -0.0082$ e/Å^2 representing the hydrogen bond donor region, $\sigma > +0.0082$ e/Å^2 representing the Hydrogen bond acceptor region and $-0.0082 < \sigma < +0.0082$ e/Å^2 indicating the non-polar region. Sigma surfaces were also generated to visualize charge densities on respective surface area of molecule.

Receptor binding pocket analysis

To determine the ligand binding sites of each receptor, we used the server POCASA (1.1) where a spherical probe (radius of 2 Å) is rolled along the surface of the protein to

find the top 5 pockets containing the higher volume of distribution (VD) [43]. Specifically, VD measures the volume depth of the pocket which is a good indicator of where the ligand is most likely to bind. The web server also offers noise points cancelation with the single-point flag and protein-depth flag parameters as well as probe size adjustment in order to have a better understanding of the shape and volume of the pocket [44].

Docking studies

Docking studies to determine ligand binding were conducted using two software. These include AutoDock Vina v.1.2.0 and HDOCK. For AutoDock Vina, v.1.2.0 the ligand and receptors were first prepared in AutoDockTools (1.5.6) and were then uploaded into AutoDock Vina v.1.2.0. The receptors were initially downloaded as a.pdb file from the RCSB Protein Databank web server. After removing the ligand from the receptors using PyMol and downloading it as a.pdb file, these were then inserted into the graphical user interface, In AutoDockTools (1.5.6), polar hydrogen bonds were added along with kolman charges and water molecules were deleted. The protein was then saved as a.pdbqt file. Then the. pdb ligand that had been designed on ChemDraw3D (20.1.1) was also individually added to the AutoDockTools (1.5.6) where it was also saved as a.pdbqt file. Lastly, both.pdbqt files were added to AutoDockTools (1.5.6). This creates a grid box in the receptor which is the area within which the binding conformation of the ligand [45] is obtained using AutoDock Vina v.1.2.0. For the receptors, we used the default coordinates (x,y,z) for the 40°A × 40°A × 40°A grid box, namely 103.237, − 4.422, 52.353 for the EphA2 kinase domain of the receptor and − 17,659, 58.284, 3.16 for ligand-binding domain of EphA2 receptor. All other parameters used were default such as exhaustiveness at 8 and energy range at 4. A command line was then used to run the command line interface AutoDock Vina v.1.2.0 which generated a table with the binding affinities of the top nine ligand binding positions. This table is then saved as a.txt file on the local computer followed by an output.pdbqt file with the most optimal binding conformation that was calculated. This file was opened on PyMoL along with the receptor to visualize the ligand-bound receptors. It has been indicated that comparison of binding interactions using multiple docking methodologies aids in improving docking predictions [46]. We therefore also used HDOCK for further validation of the results. Unlike AutoDock Vina v.1.2.0, HDOCK is not restricted to the grid box on the receptor that is selected. Instead, it requires no information about the binding site since it can automatically integrate it from the PDB. When the.pdb file of the ligand and receptor are uploaded, the web server performs a search to look for homologous sequences. Two sets of homologous templates are then compared [47]. If there are common records, a common template is generated otherwise the best template is selected. Then global docking is performed to determine the best binding conformations [48].

Binding interactions using protein–ligand interaction profiler

Once the binding affinities were obtained using docking studies, we selected the six most optimal terpenes and their conjugates and utilized the web server, PLIP (Protein–Ligand Interaction Profiler), to determine the interactions and residues responsible for the receptor-ligand binding [49]. To prepare the file for PLIP, we opened the output.pbdqt file that was generated from *AutoDock Vina* v.1.2.0 and the receptor.pdbqt file saved from AutoDockTools (1.5.6) on PyMOL (2.5.2). That file containing the best binding poses of the ligands on the receptor was then exported and saved as .pdb file and uploaded to the web server PLIP. The results were generated as a.txt file with all the non-covalent interactions as well as the specific residues involved in binding as well as.pdb files for visualization on PyMOL [50].

Molecular dynamics simulations

To determine the stability of the ligand-receptor complexes, we conducted molecular dynamic studies using DESMOND through the Schrodinger's Maestro program (v. 2020–4) [51]. The parameter assignment for OPLS3e force field was performed using Schrodinger Maestro in two steps. First, each output.pdbqt file from AutoDock Vina v.1.2.0 was transferred to PyMOL and exported as.mae file. Those files were then imported to Schrodinger's Maestro. The first step was to prepare the protein using the Protein Preparation Wizard within Maestro to ensure structural accuracy such as complete side chains, addition of hydrogen atoms and disulfide bonds between sulfurs in close proximity followed by optimization to ensure correct hydrogen orientation in hydrogen bonding network as well as histidine rings, and asparagine and glutamine terminal amide side chain orientations [52]. The ligand was then incorporated with the receptor on the workspace where an orthorhombic boundary box with dimensions 10 Å × 10 Å × 10 Å at the predefined solvent model SPC was created around the receptor for the simulation to be performed with DESMOND. Water molecules were added to mimic aqueous conditions. Counter ions were also added to neutralize the net charge of the system (Na^+ and Cl^-). These ions can shield the charged side residues of the protein, thereby decreasing electrostatic interactions between neighboring regions of the protein. Similar MD simulations, where salt ions have been included, for

various peptides and proteins [53] to counteract electrostatic interactions have been discussed in previous works [54]. Furthermore, according to the particle mesh Ewald (PME) method, it has been shown that the simulation system must be made neutral for efficient long-range electrostatic calculations using fast Fourier transformation method. This neutral system, however, may not represent the counter ion distribution found in cellular/in vitro systems [55]. The OPLS3e force field-based torsional parameters were developed from low energy conformers and used as the starting geometries in QM optimization. Torsional parameters in OPLS3e are denoted by a truncated Fourier series similar to the OPLS3 force field as summarized in [56]. The stretching and bending components were fit to quantum chemical data. Restrained optimization of the molecules at the B3LYP/6-31G* level [57] for each discretized value of the dihedral angle was carried out. Single-point M06-2X/cc-pVTZ(-f) calculations were then used to resolve the reference energy surface [58]. Maestro provides an automated version of the fitting protocol, which was utilized to generate the parameters. The simulations were run with an NPT ensemble class to equilibrate the system at 300 Kelvin and 1.01325 bar. The "Relax model system before simulation" was selected for a series of minimizations to be performed prior to the simulation in order to relax the system. All simulations were set up to be 100 ns with 1000 frames to be recorded to the trajectory. Once simulations were completed, the -out.cms file generated from DESMOND was opened on Simulation Interaction Diagram Panel on Maestro where the data was studied. To ensure reliability and consistency, each system was simulated thrice keeping all of the run conditions the same. The values reported are averaged.

Prediction of LogP values

Since the goal is to develop drug candidates to target overexpressed receptors in tumor cells, logP values of the conjugates are important to be evaluated. For this analysis, we used ADMETlab 2.0 which utilizes quantitative structure–property relationship (QSPR) models trained by the multi-task graph attention (MGA) framework [59]. The logP value [60] provides information about the lipophilicity of the drug candidates.

Synthesis

Based on the results of MD simulations and Docking studies, as a proof of concept, we synthesized six conjugates that showed relatively high binding affinities with the EphA2 receptor. These include the MA and OA conjugates with YSAYP, VPWXE, and SWLAY. To prepare each conjugate, either MA or OA (0.053 M) was dissolved in dimethyl formamide (DMF) at room temperature. Previously established amide coupling methods were utilized [61]. To activate the carboxylic acid group of each compound, *N*-hydroxysuccinimide (NHS) (0.05 M) and 1-ethyl-3-(-3-dimethylaminopropyl) carbodiimide hydrochloride (EDAC) (0.05 M) were added. The reaction mixture was shaken at 200 rpm for 1 h at 4 °C. Then 0.06 M of either YSAYP or VPWXE (side chain of E protected with methoxy group) or SWLAY were added to the mixture and allowed to shake for 24–48 h at 4 °C. After completion of reaction, the solvent was rotary evaporated and the product was allowed to dry overnight. In the case of VPWXE conjugate, the ester group was removed by base hydrolysis and then recrystallized with acetone. The formation of products was confirmed by ^{1}H NMR spectroscopy conducted using a Bruker 400 MHz NMR spectrometer. The solvent utilized in all cases was DMSO-d6 with 0.03% TMS. Results of the NMR analysis are given in Supporting Information.

Cell studies

We examined the interactions of the conjugates with two different cell lines namely F98 (ATCC CRL-2397) rat undifferentiated glioma cells which are known to overexpress EphA2 receptors [62]. To assess, if there was any effect on non-cancer cell lines, we also examined the interactions of the conjugates and the peptides with fibroblasts (C57BL/6 ATCC SCRL-1008). The F98 cells were grown to confluence in RPMI medium, supplemented with 10% fetal bovine serum (Thermofisher Scientific), 1% 10,000 I.U./mL Penicillin, 10,000 (µg/mL)100 units/mL streptomycin, while the fibroblast cells were grown in DMEM containing 10% FBS, 1% 10,000 I.U./mL Penicillin, 10,000 (µg/mL)100 units/mL streptomycin. Each cell line was grown as monolayers in a humidified atmosphere at 37 °C in a 5% CO_2 incubator. The media was changed every 2 days and the cells were split once or twice a week.

Cell viability and morphology studies

To examine cell viability, we plated cells at a density of 1×10^4 cells/well in 96-well Falcon polystyrene tissue culture plates. After allowing the cells to spread and attach for 3 h, we added three different concentrations of each of the assemblies to the cells to examine their effects at varying concentrations. Specifically, we tested 2.5 µg/mL, and 5.0 µg/mL and 9.5 µg/mL concentrations of the assemblies. The growth of the cells was monitored over a period of 24 and 48 h. To determine cell viability, we performed WST-8

assay [63]. The absorbance at 480 nm was monitored at each time point using a BioTek Eon microplate reader. Triplicate experiments were run in all cases. The absorbance of media with no cells was used at the blank and was subtracted from all samples. Percent cell viability was calculated according to the formula [(O.D of cell plus scaffolds)/(O.D of cells alone)] × 100. Then standard deviations were calculated. Statistically significant differences were then determined using student's *t* test. Cells were imaged using an inverted Amscope IN480TC-20MB13 at various magnifications to determine the effects on cell morphology.

Apoptosis assay

To gain further insight into the mechanism of cell death induced by some of the conjugates, we performed apoptosis assay. Cells were plated at 80% confluence on a 24-well Falcon polystyrene tissue culture plate at a density of 1.9×10^5 cells/well. The cells were then incubated at 37 °C in a 5% CO_2 incubator for 3 h to adhere and spread. The conjugates were then added to each well at varying concentrations (2.5 µg/mL, 5 µg/mL, and 10 µg/mL). After an incubation period of 24 h, Annexin V FTIC-Propidium Iodide Assay was performed [64]. The stage of apoptosis was then evaluated by fluorescence microscopy using an inverted Amscope IN480TC-20MB13. Green fluorescence is seen due to the dye FTIC that is conjugated to annexin which has a high affinity to phosphatidylserine. When the cell is in early apoptotic stages, the phosphatidylserine becomes exposed on the outer leaflet of the outer membrane allowing annexin V to bind and FTIC to fluoresce [65]. Red fluorescence on the other hand is indicative of late apoptosis or necrosis as the dye, propidium iodide must pass through the disrupted membrane in order to bind to the DNA of the cell and fluoresce [66].

ADP Glo assay

To confirm whether the OA and MA peptide conjugates with SWLAY, YSAYP, and VPWXE showed any inhibitory activity with EphA2 kinase, we performed an ADP-Glo Kinase Assay [67]. Prior to the actual assay, we optimized the concentrations of kinase and kinase substrate. To determine the optimal substrate concentration, a serial twofold dilution of kinase substrate (Poly (Glu, Tyr) sodium salt) was prepared in kinase buffer (containing 40 mM Tris at pH 7.5, 20 mM $MgCl_2$, and 0.1 mg/mL) using 10 µg/mL of kinase and 80 µM of ATP. After an incubation period of 2 h, the ADP-Glo reagents were added, and the luminescence was read using a Biotek SynergyH1 microplate reader. It was determined that the optimal concentration of the kinase substrate was 2 µg/mL. To determine the optimal kinase concentration, a twofold dilution of kinase was prepared in kinase buffer and added to 80 µM ATP and the optimal concentration of substrate that had been determined previously. After incubating and adding the ADP-Glo reagents, the luminescence was read and plotted (data not shown). The optimal kinase concentration determined was 6 µg/mL.

Once the concentrations of the kinase enzyme (EphA2) and kinase substrate had been determined, we conducted the kinase reaction assay. This was done by creating a twofold serial dilution of the different inhibitors which were incubated at concentration range of 0.18 µM to 30 µM in a white 96-well plate, starting with 5 µL of 50 µg/mL solution, and diluting it until the appropriate concentration was reached. The same volumes of 2.5X the optimal concentration of kinase and kinase substrate were then added to each well, followed by 10 µL of 80 µM ATP. The control wells were prepared under the same conditions except DMSO was utilized. The contents of the well plate were then shaken in the Gennie Temp-Shaker 300 at 120 rpm for 2 min and then incubated at room temperature for about 2 h.

After the incubation period, the assay was started by adding 25 µL of ADP-Glo reagent. This reagent terminates the reaction by depleting all of the ATP that had not been cleaved by the KBD of EphA2. After an incubation period of 40 min at room temperature, the Kinase Detection Reagent was added to convert all of the ADP that had been created back to ATP in order to generate luminescence through a luciferin reaction. After 30 min, the luminescence was read using a BioTek SynergyH1 microplate reader at an integration time of 0.5 s and a gain of 255. The luminescence corresponds to the amount of ADP that was generated from the reaction, thus giving the kinase activity in presence of inhibitors.

Surface plasmon resonance analysis

To further explore the binding interactions of the EphA2 receptor with the most optimal conjugate (oleanolate-SWLAY), we conducted surface plasmon resonance studies with both the kinase-binding domain (amino acids Leu 585-Ile 976 His & GST tag, Sino Biological) and the ligand-binding domain (amino acids Met 1-Asn 534, His tag Sino Biological) of the receptor. In addition, we also conducted surface plasmon resonance (SPR) analysis with positive controls for each domain (Recombinant Human Ephrin A1 Fc tag, Sino Biological) for the ligand binding domain and the commonly known kinase inhibitor drug Dastanib (Selleckchem) with the kinase binding domain. To begin, gold chips (Platypus technologies, Biosensor chip SF-10 glass (index = 1.72)) were washed with 70% ethanol and were irradiated with UV light for 10 min. These were then coated with a stock solution of 11-mercaptoundecanoic acid (1 M in ethanol) to functionalize the chips. After an hour, the carboxylic group of 11-mercaptoundecanoic acid was activated using *N*-hydroxysuccinimide (NHS) (0.01 M) followed by

EDAC (0.01 M). The gold chips were incubated for another hour. Then the respective EphA2 receptor protein (either kinase-binding domain or ligand-binding domain) was incubated on the gold chip at a concentration of 2 µg/mL at 4 °C for 24 h. Before starting the study, the chip was placed on the flow cell and one drop of Cargill's 7.21 index fluid was added to the opposite side of the chip where the SPR prism was placed. The system was then allowed to stabilize with 1X PBS buffer solution. Once the system was stabilized, each specific analyte was then introduced into the system. The binding kinetics of each analyte was tested at room temperature at a concentration range of 25 ng/mL to 100 ng/mL. On average, each run was carried out for 2200 s. The flow-rate was kept constant at 30 µL/min. Each run was carried out in triplicate. To determine the KD of each sample, the data obtained was then input into the software GraphPad Prism and non-linear regression analyses were carried out.

Statistical analysis

All studies were carried out in triplicate. Student's *t* test method was used to determine statistically significant differences.

Results and discussion

Sigma profiles

To predict the physicochemical properties of the terpenes, their peptide conjugates, and the three neat peptides, we utilized the software COSMO-RS, which uses information about the conductor surface polarization charge densities σ as indicated in the conductor-like screening model of realistic solvation (COSMO-RS). The graphs obtained for the surface polarities essentially signify the sigma profiles, which can provide vital information regarding partition and adsorption coefficients which are key to examining "drug-like" properties of the various conjugates [68]. Results obtained are shown in Fig. 2. As shown in Fig. 2a, the terpenes displayed varying amounts of hydrophobicity as indicated by the peaks in the neutral region (σ value ~ 0 e/A^2) due to their cyclic terpenoid composition. OA was the most hydrophobic compound due to the lesser number of hydroxyl groups compared to MA and HB. All three of the terpenes are pentacyclic terpenoids. HB and MA on the other hand possess additional hydroxyl groups, thus making them relatively less hydrophobic. PA is unique as it possesses a furano-diterpene structure [69] making it least hydrophobic. LA possesses more hydrophobic character compared to polyalthic as it lacks the furan ring system. QA has a unique structure due to the bridged structure in addition to the carbonyl groups of the quinone like ring system. The peaks in the hydrogen bond donor (HBD) region are attributed to the carboxyl groups that are found in all of the terpenes studied here, as well as the presence of the hydroxyl groups found in HB, MA, and OA. The latter is responsible for HB, MA, and OA, respectively having higher peaks in this region. The peaks in hydrogen bond acceptor (HBA) regions (positive σ values) are attributed not only to the presence lone pair of oxygen. As expected, PA had a relatively higher peak at a sigma value of + 0.015 e/A^2 due to the furan ring system, which confers the molecule π H-bond acceptor properties [70]. The sigma profiles and corresponding sigma-surfaces of the conjugates and the individual peptides are shown in Fig. 2b–d. As shown, all conjugates showed an increase in the values in HBD and HBA regions due to the incorporation of the peptide moieties containing amide groups as well as the new amide bond formed between the terpene moiety and the N-terminal of each of the peptides. An increase was also observed in the hydrophobic region; however, the trends were similar to unconjugated terpenes. Thus, the OA-peptide conjugates had the highest hydrophobicity while the PA peptide conjugates had the lowest hydrophobic character regardless of the peptide that was conjugated. This increase in hydrophobicity is due to the fact that the peptide moieties contain hydrophobic residues such as two tyrosines, one alanine and one proline for YSAYP, though serine adds hydrophilic character due to its –OH group. In the case of the SWLAY conjugates, except for serine, once again all of the residues are hydrophobic, and in the case of VPWXE, the case is similar with E being the only non-hydrophobic residue. Interestingly, the sigma-plots in the H-bond donor region showed relatively higher peaks in the H-bond donor region for the YSAYP conjugates due to the incorporation of three additional hydroxyl groups (two from Tyr and one from Ser) while the SWLAY conjugates lead to two additional –OH groups and the VPWXE lead to the addition of the side chain –COOH of the glutamic acid residue. The C-terminal carboxyl group was free for all conjugates as well, leading to an overall increase in the peak intensities in the H-bond donor (HBD) regions. Compared to the conjugates each of the peptides had lowest hydrophobicities due to the absence of the terpene moieties. These results indicate that the conjugation of the peptide sequences to the terpenes enhanced the H-bond donor and H-bond acceptor (HBA) capabilities while also increasing the hydrophobicity which may be important in cell-permeation and receptor binding. We also designed conjugates with a linker attached to the terpenes and the peptides. The linker utilized was 5-amino valeric acid, leading to the formation of an amphiphilic conjugate with four carbons (C4) separating the peptides from the terpenes. Results for the MA and OA conjugates with C4 linker are shown in Supplementary Information (Fig. S2). Results show that, compared to the conjugates without the linkers, the conjugates with linkers had higher

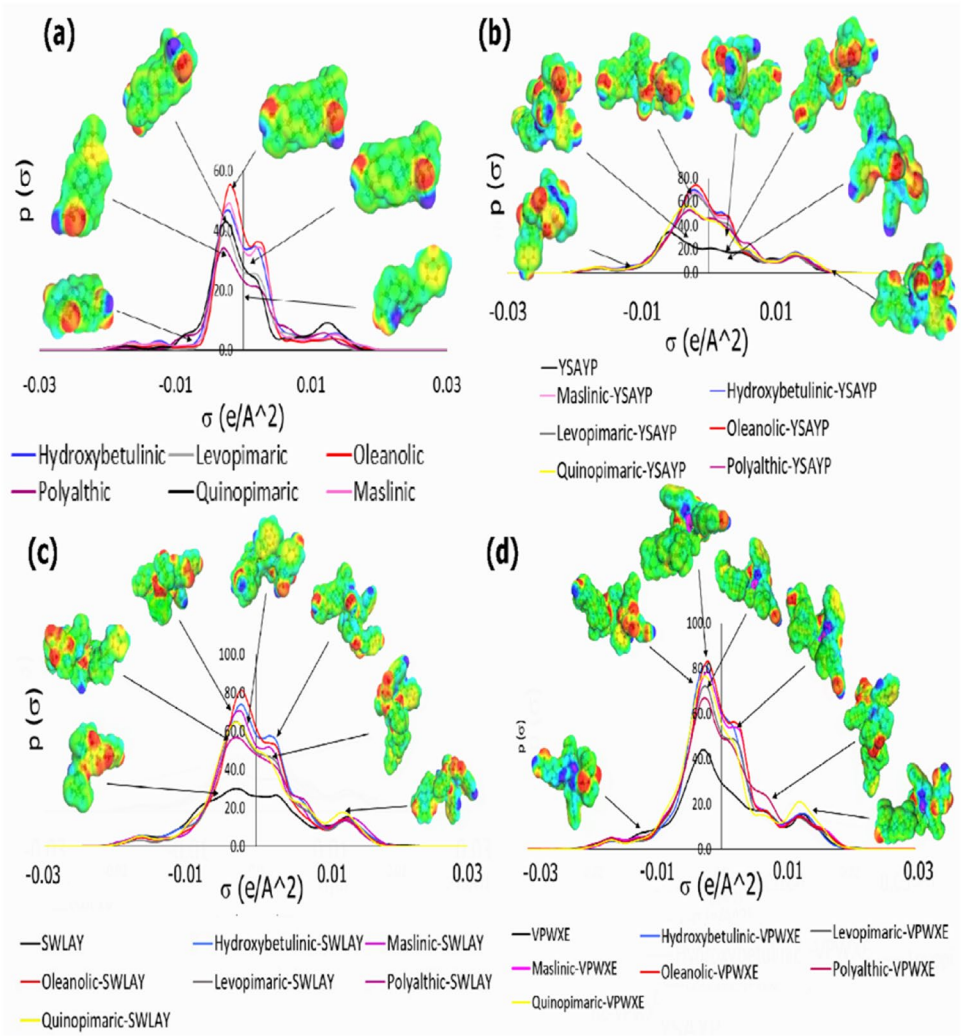

Fig. 2 σ-Profiles and sigma surface of compounds. **a** Terpenes; **b** YSAYP and conjugates with each of the terpenes; **c** SWLAY and its conjugates with each of the terpenes; **d** VPWXE and each of its conjugates with each terpene. For the sigma surfaces, red color indicates H-bond acceptor region, green/yellow indicates hydrophobic/neutral; blue color is indicative of H-bond donor region

hydrophobicity as indicated by the peak between − 0.0082 e/Å^2 and + 0.0082 e/Å^2. Of these, OA-VPWXE-C4-linker conjugate had the highest hydrophobicity while the MA-YSAYP-C4-linker conjugate had the lowest hydrophobicity. All the linker conjugates also showed a slightly more pronounced peak in the HBD and HBA regions due to the additional amide bonds that were introduced.

Binding pocket analysis

It is crucial to study the binding pockets of the receptors to determine the locations of preferred binding regions within each of the receptors. The receptors studied here include EphA2 kinase domain (PDB ID: 5NK1) [71] and EphA2 ligand binding domain (PDB ID:3C8X) [72]. The results obtained are shown in Fig. 3 and Table 1. The webserver POCASA was used to determine the binding pockets. In the case of the EphA2 receptor kinase domain, the top five pockets are shown. The highest ranked pocket had a volume distribution (VD) of 986 and with a volume of 346 Å. Furthermore, the highest ranked binding pocket was found in the ATP binding pocket involving residues Y694 and E696 located toward the ATP pocket entrance, I619 and A699 in the ribose pocket and the gatekeeper residues T692 and M695 in the hinge region [73]. The top 5 pockets were also determined for the ligand binding domain with the highest-ranking pocket having a VD of only 147 and a volume of 60 Å. This indicates that the kinase domain has a larger binding area, which may be more conducive toward binding with the peptides conjugated to the terpenes.

Molecular docking studies

EphA2 receptor (ligand binding domain)

We first utilized AutoDock Vina to determine the binding affinities of the terpenes, the peptide conjugates with YSAYP and SWLAY, as well as that of the unbound peptides. In previous work, crystal structures of the longer forms of these peptides in complex with Eph receptors [74] have shown that

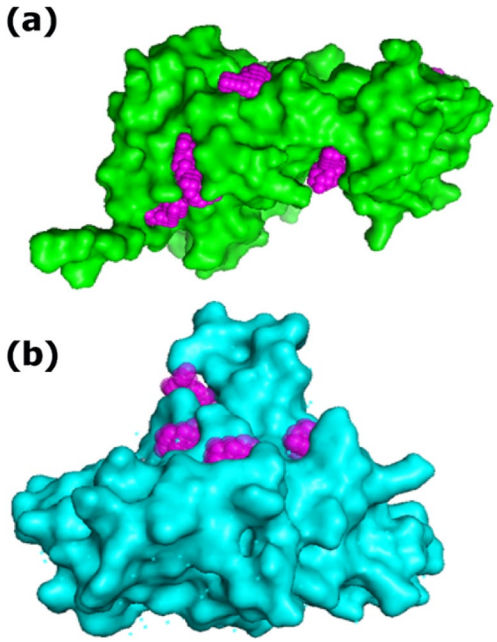

Fig. 3 POCASA results showing binding pockets of each receptor domain in magenta. **a** Ligand binding domain of EphA2 receptor; **b** kinase domain of the EphA2 receptor

Table 1 Binding pockets obtained based on POCASA results

Kinase binding domain (KBD) of EphA2			Ligand binding domain (LBD) of EphA2		
Pocket number	Volume (Å)	VD	Pocket number	Volume (Å)	VD
161	346	986	207	60	147
366	94	262	175	34	86
118	97	237	121	31	74
403	81	225	24	28	74
191	61	165			

Table 2 Binding affinities of conjugates, peptides, and terpenes using AutoDock Vina and HDOCK (without linker)

Name of the terpene or terpene-peptide conjugate	*KBD EphA2		*LBD EphA2	
	AutoDock (Kcal/mol)	HDOCK	AutoDock Kcal/mol	HDOCK
YSAYP	−7.5	−165.47	−5.4	−154.21
MA-amido-YSAYP	−10.7	−200.90	−7.8	−171.74
OA-amido-YSAYP	−9.9	−197.67	−7.6	−169.27
QA-amido-YSAYP	−9.9	−193.22	−7.1	−181.62
LA-amido-YSAYP	−9.7	−180.47	−5.8	−180.08
HB-amido-YSAYP	−8.7	−199.20	−7.2	−198.11
PA-amido-YSAYP	−8.7	−187.40	−4.7	−174.06
SWLAY	−8.5	−198.01	−6.1	−169.29
OA-amido-SWLAY	−10.5	−191.39	−7.0	−173.8
QA-amido-SWLAY	−10.1	−193.75	−7.9	−186.80
MA-amido-SWLAY	−10.1	−185.98	−6.4	−172.80
LA-amido-SWLAY	−9.8	−182.36	−7.4	−179.67
PA-amido-SWLAY	−9.5	−184.15	−7.4	−182.87
HB-amido-SWLAY	−9.3	−204.98	−7.2	−179.75
VPWXE	−7.8	−170.82	−6.5	−159.90
HB-amido-VPWXE	−9.6	−190.16	−5.9	−180.67
QA-amido-VPWXE	−8.8	−198.98	−7.0	−178.52
OA-amido-VPWXE	−8.6	−186.47	−6.3	−187.90
MA-amido-VPWXE	−8.6	−187.74	−6.2	−186.15
LA-amido-VPWXE	−8.5	−182.78	−6.9	−173.87
PA-amido-VPWXE	−7.6	−192.00	−6.4	−172.58
QA	−9.1	−158.60	−6.7	−129.08
OA	−8.9	−134.63	−7.4	−125.42
MA	−8.4	−141.48	−7.2	−130.07
LA	−8.4	−134.03	−6.0	−101.02
HB	−7.9	−146.09	−7.1	−121.74
PA	−7.6	−132.64	−5.9	−106.12

* *KBD* kinase binding domain, *LBD* ligand binding domain

the peptides bind in the hydrophobic ligand-binding channel. The flexibility of the receptor loops that comprise the ligand-binding cavity allow for an induced-fit mechanism [75]. As seen in Table 2, the AutoDock results indicated that compared to the peptide YSAYP, the binding affinity increased upon conjugation with the terpenes with the exception of the conjugate comprising the PA moiety. In the case of the SWLAY conjugates, similar results were observed. For the VPWXE conjugates however, with the exception of LA and QA-amido VPWXE conjugates, a slight decrease in binding affinity was observed compared to the unbound peptide. To further validate these results, we utilized a second docking server, the HDOCK server. This server utilizes a hybrid docking strategy and automatically incorporates binding interface information into normal global docking and uses intrinsic scoring functions to provide a docking score [76, 77]. Based on HDOCK results, though the general trends were similar as there was an increase in binding score upon conjugation with the terpenes, slight differences were seen. For example, HDOCK showed an increase in binding score for PA-amido-YSAYP compared to YSAYP, while AutoDock Vina showed a slight decrease in binding affinity. This trend was also seen in the case of some of VPWXE conjugates. These differences arise due to the variations by which calculations from each software are carried out and are reported. Unlike HDOCK, AutoDock Vina uses algorithms that search for the conformation of a flexible ligand by a global optimization of the scoring function. During this process, the ligand binding score is determined by an empirical scoring function, which consists of the following equation $\Delta G = Ws_1\ gauss_1 \times Ws_2\ gauss_2 + WR$

Repulsion + Whp × Hydrophobic + Whb × HB + WrotNrot, which takes into account van der Waals interactions, hydrophobic and H-bonding interactions, as well as torsional entropy loss upon binding [78, 79]. Thus, overall from docking results, one can conclude that in most cases, the binding is enhanced upon conjugation.

We also compared the docking results with that of the unbound terpenes which indicated that the binding affinities of the peptide bound conjugates were comparable with that of the neat terpenes, though LA-amido YSAYP and PA-amido YSAYP and MA-SWLAY showed a slight decrease in binding affinity according to AutoDock results. Overall, VPWXE conjugates were found to have lower binding affinities compared to SWLAY and YSAYP, which is expected given that those two peptides have been shown to be specific for binding to the LBD domain of the EphA2 receptor. HDOCK results however showed an increase in the binding score for all conjugates.

To further assess these results, we conducted PLIP analysis (Fig. 4) and Table S1 (Supplementary Information). For YSAYP, the main interactions appeared to be H-bond interactions between –OH groups of the Tyr and Ser moieties with Thr 45 and Tyr 48 and Thr 132 respectively, implying that interactions occur with the D-E region as well as the G-H region. Tyr 48 and Leu 44 are also involved in hydrophobic interactions. Upon conjugating with the YSAYP peptide, a slight shift occurs and some of the interactions seen include Gln 56, Asn 84, Tyr 87, Tyr 48, Thr 132, and Leu 44 for the HB-amido-YSYAP conjugate. For the MA and OA amido-YSAYP conjugates however, a decrease in number of H-bonds is seen (one H-bond with Leu 41 for the MA conjugate and three for the OA conjugate). Interestingly, there is an increase in hydrophobic interactions compared to the HB, for the MA conjugate. This may be due to the fact that in MA, the –OH groups are adjacent to each other, and may be involved in intramolecular H-bonds, resulting in less interactions with the receptor compared to the HB conjugate, where one of the –OH groups is part of a $–CH_2OH$ group. Interactions with Leu 48 and Tyr 48 are maintained. Additionally, while the unbound peptide and the HB and MA conjugates did not show any salt bridge formation, the OA-amido-YSAYP conjugate shows a new salt bridge with His 46.

The LA and QA-amido YSAYP conjugates show six and five H-bonds and two and five hydrophobic interactions respectively. While interactions with Leu 44, Tyr 48, and Thr 132 are still maintained, a new interaction is observed with Arg 82 in the case of the LA conjugate and with residues Gly 42 and Phe 134 with the QA conjugate. The PA conjugate shows only two H-bonds with residues Gly 131 and Arg 82, while six hydrophobic interactions are once again seen with Leu 44, Tyr 48, and Thr 132. These results indicate that Tyr 48, Leu 44, and Thr 132 are commonly found interacting with the conjugates as well as with the peptide, and therefore play a critical role in binding with the LBD of the receptor.

Salt bridges are once again seen with Arg 82 for the LA-amido-SWLAY, QA-amido-SWLAY, and PA-amido SWLAY conjugates. Interactions are also seen with Tyr 48 in the case of the HB, OA, PA, and QA-amido-SWLAY conjugates. For MA-amido-SWLAY, Tyr 48 is involved in π-stacking interaction with the tryptophan moiety of the SWLAY. Interestingly, hydrophobic interactions with Leu 44 are not seen for the MA, OA, and the PA-amido SWLAY conjugates. However, a critical new hydrophobic interaction is seen with Tyr 65 with all SWLAY conjugates except the OA amido SWLAY conjugate. Comparatively, MA and OA-amido SWLAY conjugates had lower number of hydrophobic interactions while QA-amido SWLAY showed the highest number of hydrophobic interactions (seven). The highest number of H-bonds were observed with the HB-amido-SWLAY conjugate due to the $–CH_2OH$ group which further facilitates H-bonding interactions as was seen in the case of YSAYP conjugates. H-bonding interactions with Gly 42 was also found to be important in binding with several of the SWLAY conjugates and the SWLAY peptide itself. Overall, once again, most interactions were found in the D-E region and the G-H regions. The binding is promoted due to several predominantly hydrophobic contacts with Tyr 48, Tyr 65, Leu 41, Leu 44, Asn 84 in most cases. LA and PA-amido-SWLAY conjugates had additional hydrophobic contacts with Leu 54, while MA conjugates showed contacts with Val 30, Tyr 87, and Val 86 which were unique to this molecule indicating that it was binding at a slightly different position, though still within the D-E and G-H regions of EphA2 ligand binding domain.

For the VPWXE peptide, the most striking difference observed was that there were no hydrophobic interactions seen with the LBD of EphA2, which explains the relatively low binding affinity of this peptide. However, upon conjugation with the terpenes, common hydrophobic interactions were once again seen with Tyr 48, Leu 44, and Leu 41 in most cases. The OA-amido-VPWXE conjugate showed the highest number of H-bonding interactions (seven), while LA-amido-VPWXE showed no H-bonding interactions. QA-amido-VPWXE showed the highest number of hydrophobic interactions (eight) followed closely by MA-amido-VPWXE (seven). Most interactions were observed in the D-E region, with a few occurring in the G-H loop region (Thr 132, Phe 134) for QA, MA, and the OA-amido-VPWXE conjugates. Salt bridges with His 46 was seen for the OA-amido-VPWXE conjugate, while all others except MA-amido-VPWXE showed salt bridges with Arg 82.

Thus, overall from the docking and PLIP analyses, the SWLAY and YSAYP conjugates showed better interactions with the LBD domain of EphA2, compared to VPWXE and

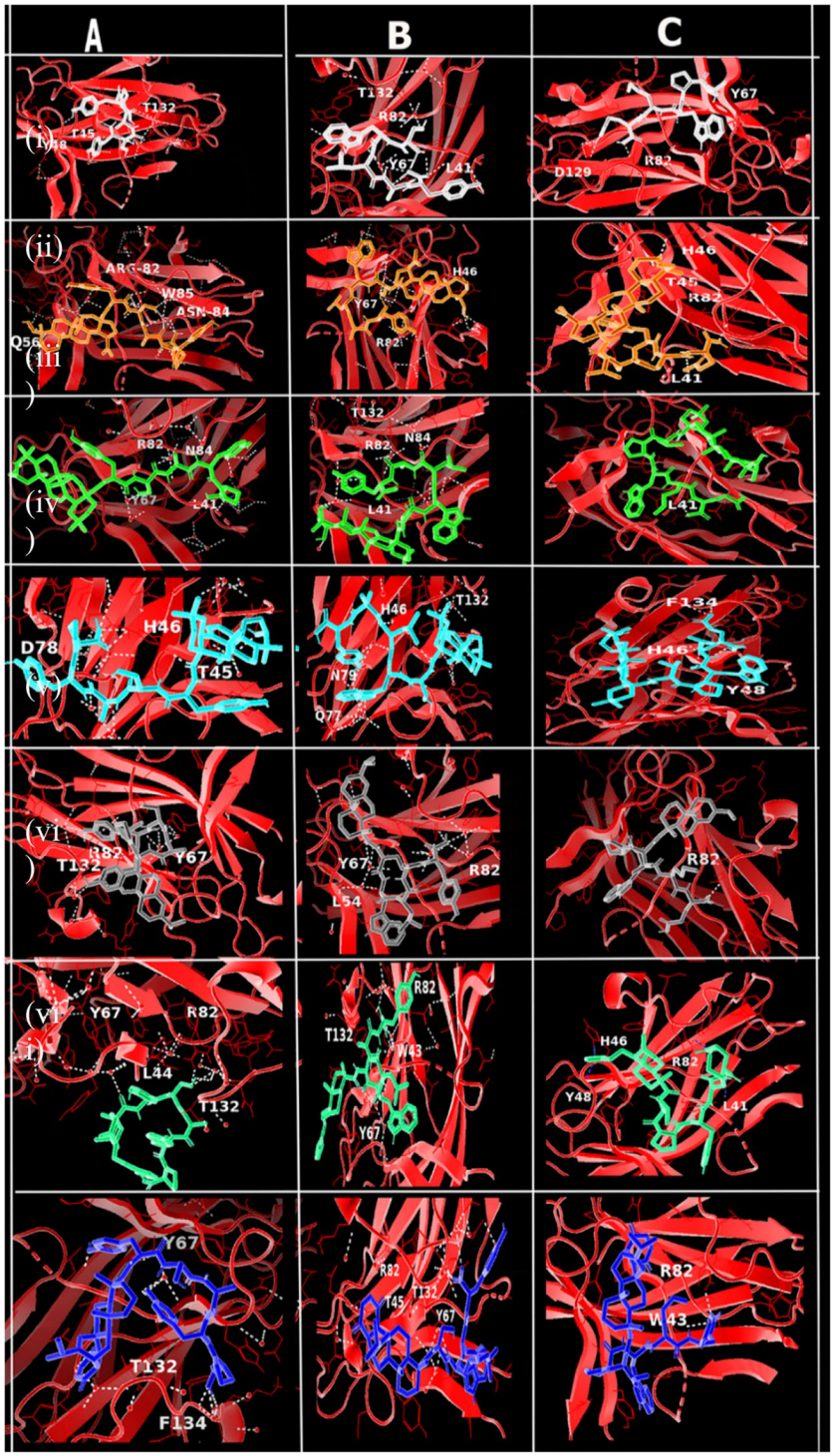

Fig. 4 *PLIP* images showing docked ligands with the ligand binding domain of EphA2 receptor. Column **A** represents YSAYP and its conjugates; column **B** represents SWLAY and its conjugates and column **C** represents VPWXE and its conjugates. Each row from i through vii indicate neat peptide; HB-conjugate; MA conjugate; OA conjugate; LA conjugate; PA conjugate; and the QA conjugate respectively

its conjugates. Hydrophobic interactions appear to play a critical role, along with H-bonding. Salt bridge formation with either His 46 or Arg 82 also played an important role in binding with these ligands. We also compared the binding interactions with the individual terpenes (Supplementary Information Table S2). Results indicated that Tyr 48 and Leu 44 were consistent residues seen interacting with all of the terpenes, which matches with the results obtained for the peptide conjugated terpenes. None of the terpenes showed any salt bridge interactions or π-stacking interactions. However, HB was found to have additional H-bond interactions with Trp 43 and Tyr 67, and was also involved in an additional hydrophobic interaction with Thr 132. LA was found to have interactions with Thr 45, and His 46 in

addition to Leu 44 and Tyr 48, which was seen for all the terpenes. Overall, the maximum number of hydrophobic interactions was observed for HB and LA (five) while all others showed two to four hydrophobic interactions. These results indicate that conjugating with the peptides enhanced interactions with the LBD of the EphA2 receptor and account for higher binding.

We then examined the impact of the C4 linker conjugates on the binding affinities with the ligand binding domain of EphA2 receptor. Results are shown in the Supplementary Information Table S3. For the ligand binding domain, the C4 linker showed mixed results compared to those obtained without the linker. While in the case of MA-amido-C4-YSAYP, QA-amido-C4-YSAYP, and PA-amido-C4-YSAYP conjugates, a marginal increase in binding affinity was observed according to docking results, (an increase of ~ 1 kcal); LA-amido-C4-YSAYP and HB-amido-C4-YSAYP showed a decrease in binding affinity while OA-amido-C4-YSAYP remained virtually the same. In the case of the SWLAY conjugates with C4 linker, most conjugates showed a marginal increase in binding affinity (between 0.3 to 1.1 kcal) with the exception of HB-amido-C4-SWLAY conjugate which showed a decrease, while no change in binding affinity was observed in the case of the PA-amido-C4-SWLAY conjugate. In the case of the VPWXE-C4-linker conjugates, results showed that most conjugates had similar binding affinities with the exception of HB-amido-C4-VPWXE, PA-amido-C4-VPWXE, and OA-amido-C4-conjugates showed an increase, while LA-amido-C4-VPWXE and QA-amido-C4-VPWXE conjugates showed a decrease. No change was observed in the case of the MA-amido-C4-VPWXE; no change in binding affinity was observed. The HDOCK scores showed that the linker conjugates showed nominal increases in most cases. Thus, it appears that the linker slightly improved the binding affinity of several of the ligands to the LBD of the receptor.

To further assess these results, PLIP analysis was conducted (Supplementary Information Table S4). For the ligand binding domain, results showed that for the HB-amido-C4-YSAYP conjugate, incorporation of the linker changed the binding interactions significantly. Without the linker, HB-amido-YSAYP binds within the D-E, J-K, and G-H region which lines the ephrin binding pocket [80]. However, upon introducing the linker, the C4 conjugate binds to the hydrophobic pocket, making contacts with residues Lys 141, Gln 183, Ile 185. All other PLIP results with the linker are discussed in the supplementary information following Table S4.

EphA2 receptor (kinase binding domain)

Similar to the ligand binding domain, AutoDock Vina results showed that upon conjugation with the YSAYP and the SWLAY, binding affinities increased for all conjugates. Interestingly, for all conjugates, the binding affinities showed higher values compared to those observed for the ligand binding domain indicating higher affinity for the kinase binding domain. A similar trend was seen with the VPWXE conjugates except for PA-amido-VPWXE where a slight decrease in binding affinity was seen upon conjugation. When comparing the results to those obtained by the HDOCK server, the YSAYP conjugates showed an increase in the scores; however, for the SWLAY conjugates, a slight decrease was observed in some cases. This is likely due to the differences in scoring methodologies as explained earlier. For the VPWXE conjugates, the HDOCK results follow the same trend as that of AutoDock Vina except that we see an increase in PA-amido-VPWXE binding affinities, which is not seen in the AutoDock Vina results. Overall, our results show that conjugation of the terpenes to the peptides increase binding affinity to the kinase binding domain of the EphA2 receptor. In all instances, the docking results from AutoDock Vina and HDOCK for the unbound terpenes also showed that conjugation with the peptides enhance the binding affinities.

These results can be explained by studies carried out using PLIP (Fig. 5 and Supplementary Information Tables S5). For the YSAYP, the main interactions that are seen include that seen between Asp 757 in the DFG motif and the hydroxyl group of Ser from the peptide. Hydrophobic interactions with Leu 746, Ala 699, Met 695, and H-bond interactions with Thr 692 occur with the between the tyrosine moieties of the peptide. Upon conjugation, the hydrophobic interaction with Leu 746 in the activation loop and hydrophobic and H-bond interactions with Ala 699 in the ribose pocket remain present with all conjugates. While it has been shown that Leu 746 is highly conserved across the kinase domains, the residue Ala 699 is important in that it drives selectivity. Other common interactions seen in the MA-amido-YSAYP conjugate and some of the other YSAYP conjugates are Asp 757 in the DFG motif of the activation loop, Ile 619 in the ribose pocket, Lys 646 in the Gly-rich loop, and Met 695 in the hinge region. Similar to the residue Ala 699, gatekeeper residue Thr 692 also confers specificity to the ATP binding site of the KBD and is also a key residue involved in drug protein interaction. Specifically, for HB-amido-YSAYP conjugate, we see a loss of interaction with Ile 619; however, H-bond interactions with Tyr 735, His 737, Asn 744, and Gly 759 arise due to interactions of the peptide fragment of the conjugates with the C-lobe. Compared to the HB-amido-YSAYP, the MA-amido-YSAYP shows an increase in both hydrogen and hydrophobic bonds; eight and nine respectively versus seven and five for HB conjugate. Due to the similarity between the structure of MA and OA terpenes, these two moieties are interacting with the same residues of the receptor namely, Lys 702, Ala 699, and Ile 619. The MA-amido-YSAYP is

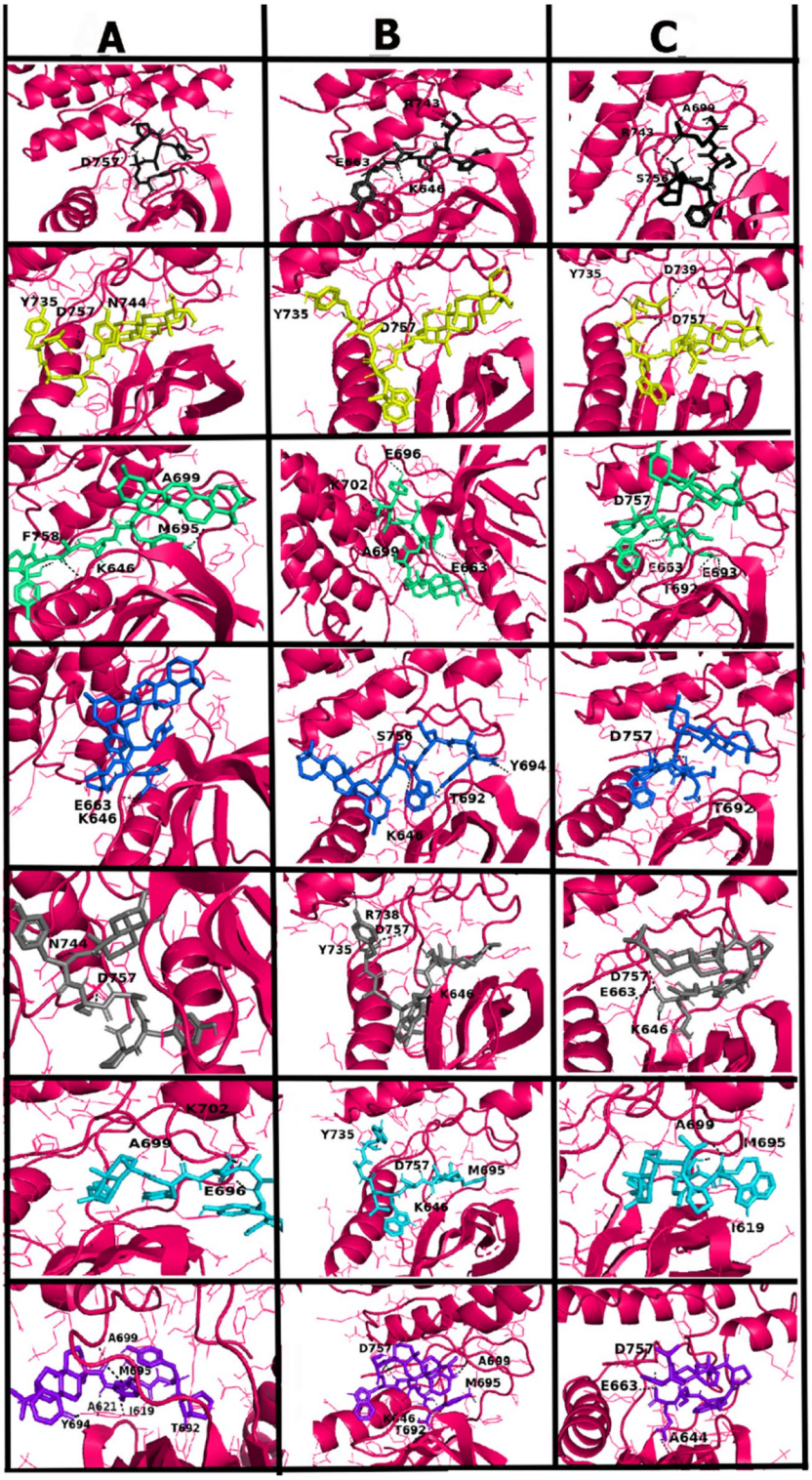

Fig. 5 *PLIP* images showing docked peptide conjugates with the kinase binding domain of EphA2 receptor. Column **A** represents YSAYP and its conjugates; column **B** represents SWLAY and its conjugates and column **C** represents VPWXE and its conjugates. Each row from i through vii indicate neat peptide; Hydroxybetuliniate-conjugate; MA conjugate; OA conjugate; LA conjugate; PA conjugate and the QA conjugate respectively

extending toward the Gly-rich loop whereas the OA-amido-YSAYP folds back on itself with and interacts with Leu 746 bringing the two tyrosine groups in close proximity. Overall, both have the same number of hydrophobic bonds (nine) however MA-amido-YSAYP has two extra H-bond interactions whereas OA-amido-YSAYP has one salt bridge.

The LA and QA-amido-YSAYP conjugates show twelve and ten hydrophobic interactions and five and ten H-bond interactions respectively in addition to one pi-stacking interaction with Phe 624 for the LA-amido-YSYAP conjugate. In addition, while some of the key interactions remain such as Met 695 and Lys 646, the majority of the remaining bonds

are not common among each other since the terpene moieties and peptides are binding to relatively different areas of the receptor. For example, one end of the QA-amido-YSYAP conjugate the carbonyl groups of ring E, of the quinopimaric moiety is seen interacting with Tyr 694 in the ATP binding pocket, while for the LA moiety part of its conjugate is binding to Leu 746 in the activation loop. PA-amido-YSAYP has the lowest binding affinity while also having distinct interactions. While interactions with key residues are maintained, two new interactions are observed with the PA-YSYAP conjugate, namely a salt bridge with Lys 629 and a pi-cation interaction with Lys 617 placing the proline moiety pointing toward the N-lobe of the receptor, where no other conjugate is binding.

The key residues for the YSAYP conjugate are still present in the SWLAY conjugate. For example, the interaction with Lys 646 that interacted with all the YSAYP conjugates is also interacting with all the SWLAY conjugates. In addition, while Asp 757 which is part of the DFG motif was also found to interact with all of the SWLAY conjugates. Similarly, Ile 619 and Met 695 are also present with most of the SWLAY conjugates. Interestingly though, the key residue Ala 699 is only present in the QA-amido-SWLAY and MA-amido-SWLAY conjugates. All the SWLAY conjugates interact with Phe 624, and with the exception of MA-amido-SWLAY, all conjugates also interact with Phe 660 as well. MA-amido-SWLAY has eleven hydrophobic interactions, eight H-bonds, one pi-cation interaction, and one salt-bridge. The salt bridge introduces an interaction that is only present for this conjugate occurring with the terminal tyrosine indicating that this conjugate is extending into a region in the receptor where the other SWLAY conjugates do not interact. The OA-amido-SWLAY conjugate has more hydrophobic interactions than the MA conjugate; however, the number of H-bond interactions is less and it also has two pi-cation interactions with Lys 646 and the tryptophan moiety which stabilize the ligand further. In fact, previous studies have shown that cation interactions are among the strongest residue-residue interactions and are less likely to be affected by solvation environment which justifies its high binding affinity [81]. QA-amido SWLAY on the other hand has the most hydrogen bonds. The two carbonyl groups from the E-ring of the QA moiety contribute to this as it interacts with the Ala 621 in the Gly-rich loop and Ala 699 in the ribose pocket. Other key interactions are maintained such as Lys 646, Asp 757, Met 695, Thr 692, and Ile 619. In fact, its high binding affinity can be attributed to the number of interactions with the key residues as well as the salt bridge and pi-stacking. LA and PA-amido-SWLAY conjugates have the same number of hydrophobic interactions while PA-amido-SWLAY has one extra H-bond and pi-stacking interaction (Phe 660), whereas LA conjugate forms a salt bridge (His 737). The HB conjugate is also pointing the terminal tyrosine in the same direction as the LA and PA-amido-SWLAY conjugate. For all three of those SWLAY conjugates, the terminal tyrosine residues are interacting with Arg 738, whereas only the LA and PA-amido-SWLAY conjugate are also interacting with Asp 739. HB-amido-SWLAY conjugate instead forms an extra H-bond with Arg 738. The tryptophan moiety of HB and PA-amido-SWLAY conjugates show interactions with Phe 660, Leu 648, Phe 624, and Gln 656. This shows that the peptide region for these 3 conjugates are binding near the same region.

For the VPWXE peptide, there is no striking difference observed compared to the other peptides. In fact, we still observe key interactions with Lys 646 in the Gly-rich loop; gatekeeper residue Thr 692, Asp 757, and Leu 746 in the activation loop; and Ala 699 in the ribose pocket. Since all the VPWXE conjugates are forming interactions with these residues located throughout the ATP binding pocket, it indicates that all the conjugates are binding relatively to the same area of the receptor. QA-amido-VPWXE conjugate showed the highest number of H-bonds (9) followed closely by the PA conjugate with eight. All the conjugates had a similar number of hydrophobic interactions with the neat peptide, HB and the QA having ten and MA and OA-amido-VPWXE conjugate having nine. PA-amido-VPWXE on the other hand only had four hydrophobic interactions. Salt bridges with Lys646 were common among MA (one), OA (two), and QA-amido-VPWXE (two) conjugates, as well as with Lys 702 and the neat peptide as well as His 737 and the HB-amido-VPWXE conjugate. Two pi-stacking interactions were also seen between the tryptophan moiety of hydroxybetulinic-amido-VPWXE conjugate and Phe 624 and Phe 660.

We then compared the binding affinities with the EphA2 kinase domain upon incorporation of the C4 linker into the conjugates, the results of which are shown in Supplementary Information Table S3; the autodock results obtained for all of the YSAYP conjugates indicated that upon incorporation of the linker, the binding affinity was lowered in all cases marginally. For the SWLAY conjugates with the C4 linker, a similar pattern was seen. For the VPWXE conjugates however, upon incorporation of the linker, the binding affinity increased by 0.6 kcal, 0.7 kcal, and 0.8 kcal for the OA-amido-C4-VPWXE, PA-amido-C4-VPWXE, and LA-amido-C4-VPWXE conjugates respectively compared to their non-linker counterparts. All other conjugates displayed binding affinities either higher for the non-linker conjugate or the same as that of the linker conjugate. Interestingly though, the HDOCK results showed a different trend where the binding score was higher for the C4 linker conjugates in comparison with the non-linker conjugates; however, the difference was marginal. The binding interactions with the EphA2 kinase domain were further assessed through PLIP analysis as shown Supplementary Information Table S6 and discussion following the Table S6.

The results suggest that for the most part, interactions with the kinase domain of the EphA2 receptor were improved upon conjugation with the terpenes and the linker did not enhance binding for the SWLAY and the YSAYP conjugates. Additionally, the SWLAY conjugates showed better interactions compared to the other peptide conjugates especially the VPWXE conjugate which proved to have the weakest interactions compared to the others. Hydrophobic interactions appeared to play a critical role in binding to the receptor as well as H-bonds. Salt formation with Lys 646 or His 737 also showed to be an important residue to bind to receptor.

Among the neat terpenes (Table S7, Supporting Information), the highest number of interactions were seen for LA (six hydrophobic interactions), while the lowest was seen for HB (three hydrophobic interactions). Val 627 was the common interaction seen in all cases except for QA; interestingly however, no interactions were seen with Met 695 with the terpenes, and Asp 757 interaction was only observed for MA. These results further confirm that the peptide conjugates of the terpenes enhance interactions with the ATP binding pocket.

Molecular dynamics studies

We further assessed the stability of the receptor-ligand complexes for both domains of the EphA2 receptor using molecular dynamics simulations. The binding pockets of each of the receptors are distinct and provides in depth information about the stability of each of the ligands. As can be seen in Table 3, for the LBD complexed with YSAYP or its conjugates, the lowest average RMSD values are seen for the unconjugated peptide and the HB conjugate. MA-amido-YSAYP also had a relatively low RMSD value at 0.87 nm. All other conjugates had a higher RMSD value > 1.0 nm and in some cases > 2.0 nm (for PA and OA conjugates). The SWLAY peptide and its conjugates displayed comparatively lower average RMSD values with the LBD domain of the EphA2 receptor. Only the LA-amido-SWLAY conjugate and the PA-amido-SWLAY conjugates had RMSD averages > 1.0 nm while all others were below 1.0 nm. In the case of VPWXE and its conjugates, the neat peptide showed a very high average RMSD value > 3.0 nm, indicative of weak binding interactions. QA-amido-VPWXE showed the lowest average RMSD at 0.48 nm, followed by LA-amido-VPWXE and MA-amido-VPWXE conjugates showing average RMSD values ~ 0.8 nm. All other conjugates showed averages > 1.0 nm and in some cases > 2.0 nm. We also compared the interactions with each of the neat terpenes and results showed that with the exception of QA, all other terpenes had higher average RMSD values > 1.6 nm. To further decipher these results, we examined the trajectories over 100 ns simulations. It has been previously reported that the Eph-ephrin ligand binding domain contains a hydrophobic channel into which the ephrin loop inserts [72]. As can be seen (Fig. 6), in the case of the YSAYP peptide, the primary interactions occur with the G-H loop region residues Thr 132-Phe 134, although the peptide itself undergoes conformation changes overtime. In the case of HB-amido-YSAYP, additional interactions occur with the anti-parallel beta-sheets that line the hydrophobic channels, in addition to residues Asp 129 in the G-H loop region and Tyr 179 in the J-K loop regions. Interactions are also seen with Trp 85 and Tyr 87. Overall, there is very little change in the position of the ligand during the simulation process. In the case of the MA-amido-YSAYP, although interactions are initially seen with the G-H loop region, by the end of the simulation, the ligand changes position and is seen interacting with Lys 50 and Tyr 48. Similar interactions occur with the oleanolic-amido-YSAYP conjugate, though by the end of the simulation, the ligand is entirely of outside of the binding pocket, with only one interaction with the G-H loop region (Thr 132) which corroborates with its higher average RMSD value. All other interactions occur closer to the N-terminal end (Gly 42, Leu 41, and Tyr 48). The Tyr 48 interaction was also seen with the MA-amido-YSYAP conjugate. The LA-amido-YSYAP conjugate shows most of the ligand on the outside, at the beginning; however, it moves inward as the simulation progresses, with interactions occurring with residues Tyr 67 and Leu 54 in the D-E region accounting for relatively lower RMSD values.

In the case of PA-amido-YSAYP, the ligand changes positions drastically over the course of the simulation explaining its relatively high RMSD, while for QA-amido-YSAYP, interactions occur within the G-H loop region (Phe 134). In general, compared to the YSAYP conjugates, the SWLAY conjugates had lower RMSD values in most cases, with the exception of LA-amido-SWLAY where the average RMSD value increased. Among the conjugates, once again HB-amido-SWLAY showed the lowest average RMSD value signifying the most stable binding interactions, followed by OA-amido-SWLAY conjugate and the QA-amido-SWLAY conjugate which also had RMSD values within 0.6 nm. The MA-amido SWLAY conjugate also showed stable interaction with average RMSD being 0.8 nm. To further elucidate these interactions, we examined the trajectories as shown in Fig. 7. As seen in the figure, the neat unconjugated SWLAY peptide primarily binds in the D-E region with a few interactions toward the N-terminal. Upon conjugation with HB-amido-SWLAY, a new interaction is initially observed with Gly 131 in the G-H loop region, in addition to Trp 43 and Gly 42. However, over the course of the simulation, the interactions are observed in the D-E region with Tyr 67, while those with the Tyr 48 and Trp 43 are retained for most of the simulation. Significant interactions are observed with

Table 3 Average RMSD values obtained for each terpene-peptide conjugate receptor complex (without linker)

Name of compound	Ligand binding domain of EphA2 receptor (nm)		Kinase domain of EphA2 receptor (nm)	
	P-L RMSD	Cα RMSD	P-L RMSD	Cα RMSD
YSAYP	0.655	0.229	0.419	0.376
HB-amido-YSAYP	0.603	0.244	0.818	0.335
LA-amido-YSAYP	0.874	0.300	0.529	0.374
MA-amido-YSAYP	1.090	0.242	0.613	0.372
OA-amido-YSAYP	2.207	0.257	0.504	0.463
PA-amido-YSAYP	2.731	0.226	0.507	0.401
QA-amido-YSAYP	1.165	0.283	0.360	0.421
SWLAY	0.603	0.223	0.630	0.629
HB-amido-SWLAY	0.581	0.237	0.589	0.339
LA-amido-SWLAY	1.527	0.225	0.521	0.376
MA-amido- SWLAY	0.809	0.236	0.583	0.432
OA-amido-SWLAY	0.604	0.294	0.378	0.279
PA-amido-SWLAY	1.230	0.292	0.694	0.510
Quinopimartate-amido-SWLAY	0.603	0.331	0.641	0.397
VPWXE	3.184	0.245	0.289	0.309
HB-amido-VPWXE	2.536	0.269	0.324	0.306
LA-amido-VPWXE	0.829	0.326	0.680	0.329
MA-amido-VPWXE	0.809	0.236	0.525	0.304
OA-amido-VPWXE	1.448	0.301	0.465	0.336
PA-amido-VPWXE	1.350	0.275	1.209	0.342
Quinopimartate-amido-VPWXE	0.482	0.245	0.706	0.496
Hydroxybetulinic acid	3.044	0.317	0.658	0.477
Levopimaric acid	1.796	0.289	0.352	0.376
MA acid	3.136	0.265	0.897	0.535
Oleanolic acid	1.767	0.252	1.000	0.411
Polyalthic acid	1.997	0.240	0.184	0.375
Quinopimaric acid	0.792	0.232	0.933	0.534

the beta-sheet region of the receptor. In the case of MA-amido-SWLAY conjugate, a new interaction is observed with Thr 45 with the –OH group of the MA component in addition to interactions with Tyr 48 and Trp 43 in the B-C region of the receptor. Overall, the ligand remains attached to the receptor throughout the course of the simulation with very little changes in conformation.

For the OA-amido-SWLAY conjugate, strong interactions are seen throughout the course of the simulation once again between Tyr 48 in addition to Lys 50, and Asp 78 in the first 50 ns; however, toward the later part of the simulation, interactions are observed with Thr 132 which is part of the G-H loop region. Interestingly, the terpene part of the conjugate remains strongly anchored to the ligand binding domain, while the last two residues Tyr and Ala appear to move away from the receptor. These results indicate that the OA moiety strongly encourages binding interactions for this conjugate. For the LA-amido-SWLAY conjugate, although the ligand initially spreads around a large portion of the receptor, making contacts with residues such as Gly 131, Gln 56, and Thr 45, toward the end of the simulation, the ligand is barely attached and moves away from the receptor, only showing H-bonding interactions with the Tyr 65 and hydrophobic interactions with Ala 37. The entire terpene moiety part of the conjugate moves away, thus accounting for the high average RMSD value. In the case of the PA-amido SWLAY, while the ligand starts out with interactions with residues such as Tyr 48 and Thr 45, however later interactions are observed in the D-E region with residues such as Trp 52 (at 50 ns) and Leu 64 and Tyr 65 by the end of the simulation. QA-amido-SWLAY conjugate shows interactions with some residues in the G-H loop region, (Arg 82) for the most part of the simulation, in addition to interactions with Gly 42, Leu 44, and Thr 45, that allows to stabilize the conjugate within the ligand binding domain of the receptor. Thus, it appears that in the case of the SWLAY conjugates, interactions with the terpene moiety within the binding pocket plays a key role in stabilizing the binding interactions.

Among all three peptides, the highest average RMSD value was observed for VPWXE (X being norleucine residue) at 3.18 nm. However, upon conjugation with the terpenes, the

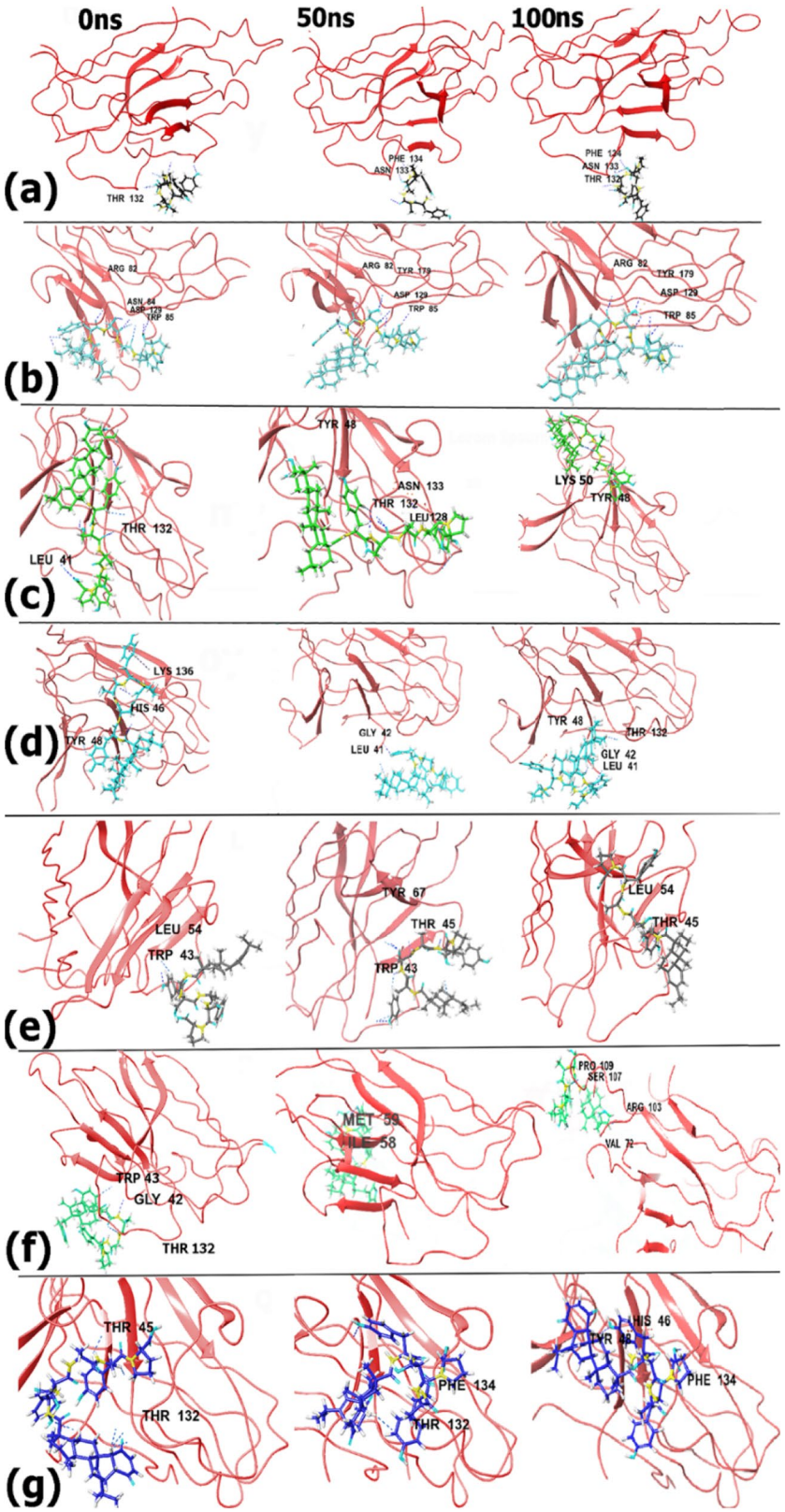

Fig. 6 Trajectory images of YSAYP and its conjugates with the ligand binding domain of EphA2 at 0 ns, 50 ns and 100 ns of the simulation (**a**) YSAYP; (**b**) HB-amido-YSAYP; (**c**) MA-amido-YSAYP; (**d**) OA-amido-YSAYP; (**e**) LA-amido-YSAYP; (**f**) PA-amido-YSAYP; (**g**) QA-amido-YSAYP conjugate

value is lowered, thus implying that conjugation with terpenes may increase interactions compared to VPWXE alone. Strikingly, among the conjugates, the HB-conjugate had the highest average RMSD value, which is opposite to the results obtained for the SWLAY and YSAYP conjugates, indicating that conjugation with VPWXE likely changes the binding

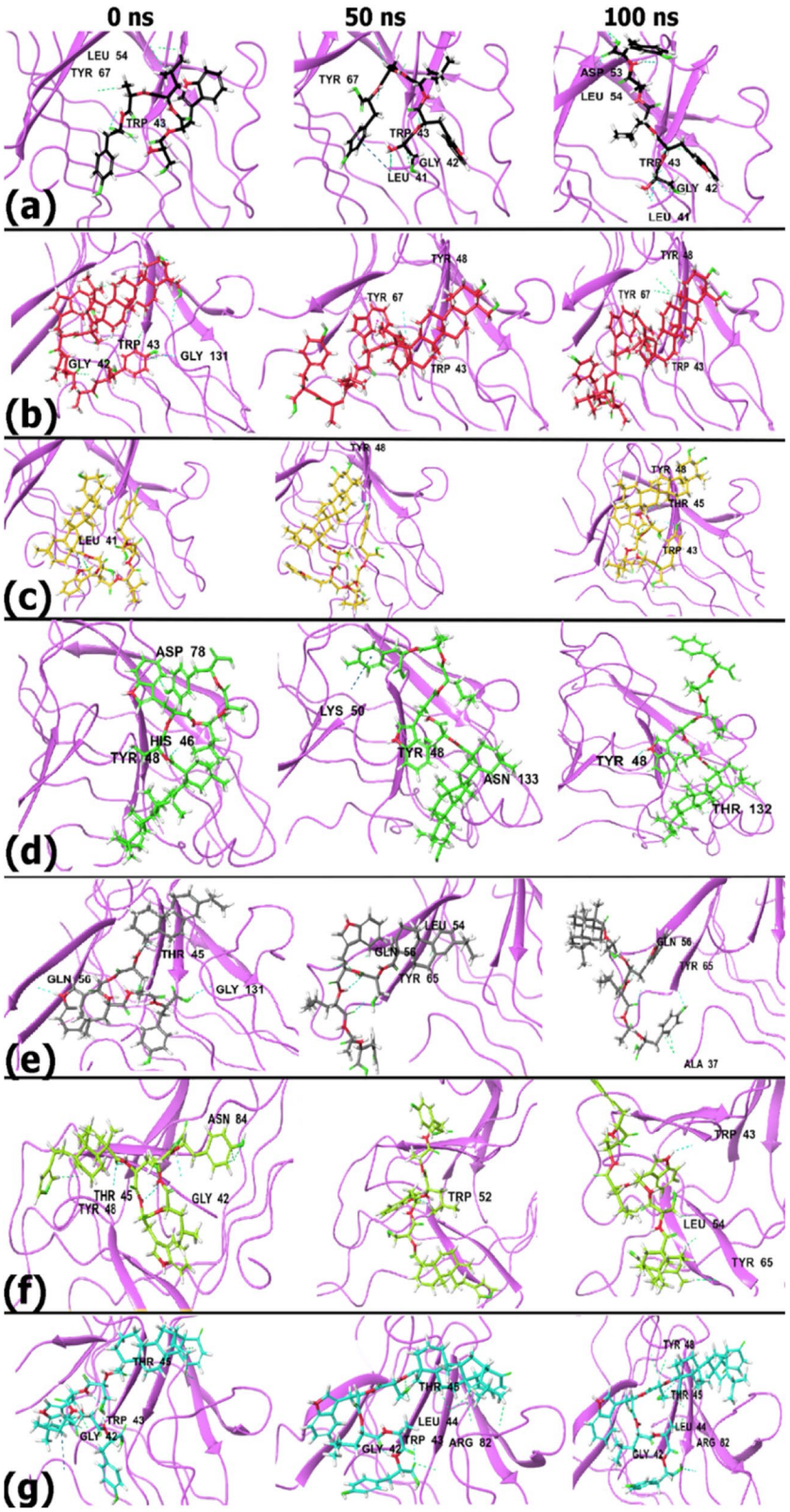

Fig. 7 *Trajectory* images of SWLAY and its conjugates with the ligand binding domain of EphA2 at 0 ns, 50 ns, and 100 ns of the simulation **a** SWLAY; **b** HB-amido-SWLAY; **c** MA-amido- SWLAY; **d** OA-amido- SWLAY; **e** LA-amido-SWLAY; **f** PA-amido- SWLAY; **g** QA-amido-SWLAY conjugate

position and reduces binding with the HB moiety. LA, MA, and QA-amido-VPWXE conjugates were the only conjugates to display RMSD values below 1.0 nm. These results are corroborated by the trajectory analysis (Fig. 8). As seen in the figure, the VPWXE peptide changes its position, and conformation during the course of the simulation significantly

and appears to move away from the receptor, with only hydrophobic interactions between Phe 95, Lys 199, and Lys 27 by the end of the simulation. Among the conjugates, for the HB-amido-VPWXE, the entire molecule appears to fold up, and move away toward the end of the simulation with interactions with Pro 63 at the end of the simulation. The MA-amido-VPWXE conjugate remains firmly attached to the receptor throughout the course of the simulation and interactions are seen between Tyr 48 and the –OH group of MA moiety. Additional interactions are also seen with Thr 45. For the OA-amido-VPWXE conjugate, multiple interactions in the G-H loop region with Gln 135, Asn 133, and Tyr 130 occur at 50 ns; however, once again by the end of the simulation, most of the ligand moves away with only interactions with Gln 36 remaining with the norleucine moiety while the terpene end is outside of the binding pocket accounting for a very high RMSD value. The LA-amido-VPWXE conjugate on the other hand remains attached to the receptor, though most interactions occur with the peptide portion, between the glutamate residue and Arg 82, a salt-bridge formation occurs and the terpene moiety is stabilized by binding with Tyr 48. Hydrophobic interactions with Leu 41 and Trp 85 are also responsible for the binding interactions.

For the PA-amido conjugate, changes occur over the course of the simulation, and interactions are seen with Phe 134 in the G-H loop region and the peptide moiety. The QA-amido VPWXE conjugate remains firmly attached in the B-C region and D-E region, with strong interactions seen with Trp 43, Leu 41, Tyr 48, and Tyr 67, implying stabilization of this conjugate primarily through hydrophobic interactions. Overall, these results indicate that of the three conjugates, a majority of SWLAY conjugates remained attached to the binding pocket of the LBD domain of the EphA2 receptor followed by YSAYP conjugates, while only three conjugates with VPWXE were found to be somewhat stable. The terpene moiety appears to be stabilized by a critical interaction with Tyr 48, which is seen interacting with almost all conjugates. Although, the significance of binding to this region needs to be further elucidated. The trajectories of the neat unbound terpenes upon interacting with the LBD of EphA2 receptor are shown in Supporting Information Fig. S3. As can be seen in the figure, with the exception of LA and QA, all other terpenes were found to move away from the receptor over the course of the simulation. Additionally, the ligands and the receptor undergoes conformational changes in all cases. These results indicate that the terpenes alone do not have stable interactions with the LBD of EphA2 and conjugation with the peptides allows for anchoring the conjugates on to the LBD. Notably, conformational changes were observed in the ligand binding domain upon binding to the various conjugates or the terpenes and peptides individually as seen from the trajectories, particularly in the loop regions.

Based on the binding affinities obtained from the docking studies, we chose to perform molecular dynamic simulations with two of the C4-linker conjugates that showed relatively higher binding affinities namely the masliante-amido-C4-peptide and OA-amido-C4-peptide. In the presence of the linker, the YSAYP conjugates showed slightly lower average RMSD value (0.7 nm and 0.8 nm) as opposed to RMSD averages of 1.0 nm and 2.0 nm obtained for the corresponding MA and OA conjugates respectively without the linker. This implies that the linker successfully enhanced interactions with the LBD for both of these YSAYP conjugates. On the other hand, introducing the linker to the SWLAY conjugates worsened the ligand-receptor stability for the two conjugates studied. The RMSD value for the conjugates without the linker averaged below 1.0 nm, whereas upon conjugation with the linker, the RMSD values were > 1.0 nm. For the VPWXE conjugate, the linker improved the ligand-receptor stability for the OA-amido-C4-VPWXE, whereas for MA-amido-C4-VPWXE the average RMSD increased, indicative of weaker interactions. The results are seen in Table 4.

To further decipher these results, we also examined the trajectories of the linker conjugates (Supplementary Information Fig. S4). The MA-amido-C4-YSAYP conjugate undergoes very little conformational change within the LBD of the EphA2 receptor. The most important contributors to this stability were the interactions with Thr 45 and Trp 43 in the N-terminal end which anchored the ligand for the entirety of the simulation. This minimal change in position corroborates with its low RMSD value. As opposed to MA-YSAYP without the linker, where there were no interactions within the G-H loop and the ligand changed conformation during the simulation. For the OA-amido-C4-YSAYP conjugate, interactions with Gly 49 as well as Thr 132 were seen in the G-H loop region throughout the simulation. As opposed to the improvement in ligand-receptor stability that was caused by the linker in the case of YSAYP conjugates, we saw weaker ligand-receptor interactions with the linker in the SWLAY conjugates. MA-amido-C4-SWLAY for example showed interactions with Leu 31 and Asp 33 for the majority of the simulation; however, unlike the results for the MA-SWLAY without the linker, the ligand is displaced entirely out of the binding pocket at the end of the simulation. Similarly, OA-amido-C4-SWLAY showed extensive interactions in the beginning of the simulation; however, toward the end of the simulation, the terpene part of the conjugate moves away from the receptor and remains anchored only by interactions with Pro 63 and Ala 37 with the peptide portion of the conjugate. This is contrary to what is seen for the compound without the linker which helps justify its lower RMSD value indicative of stronger binding interactions than that seen in the presence of the linker. The MA-amido-C4-VPWXE conjugate shows interactions with

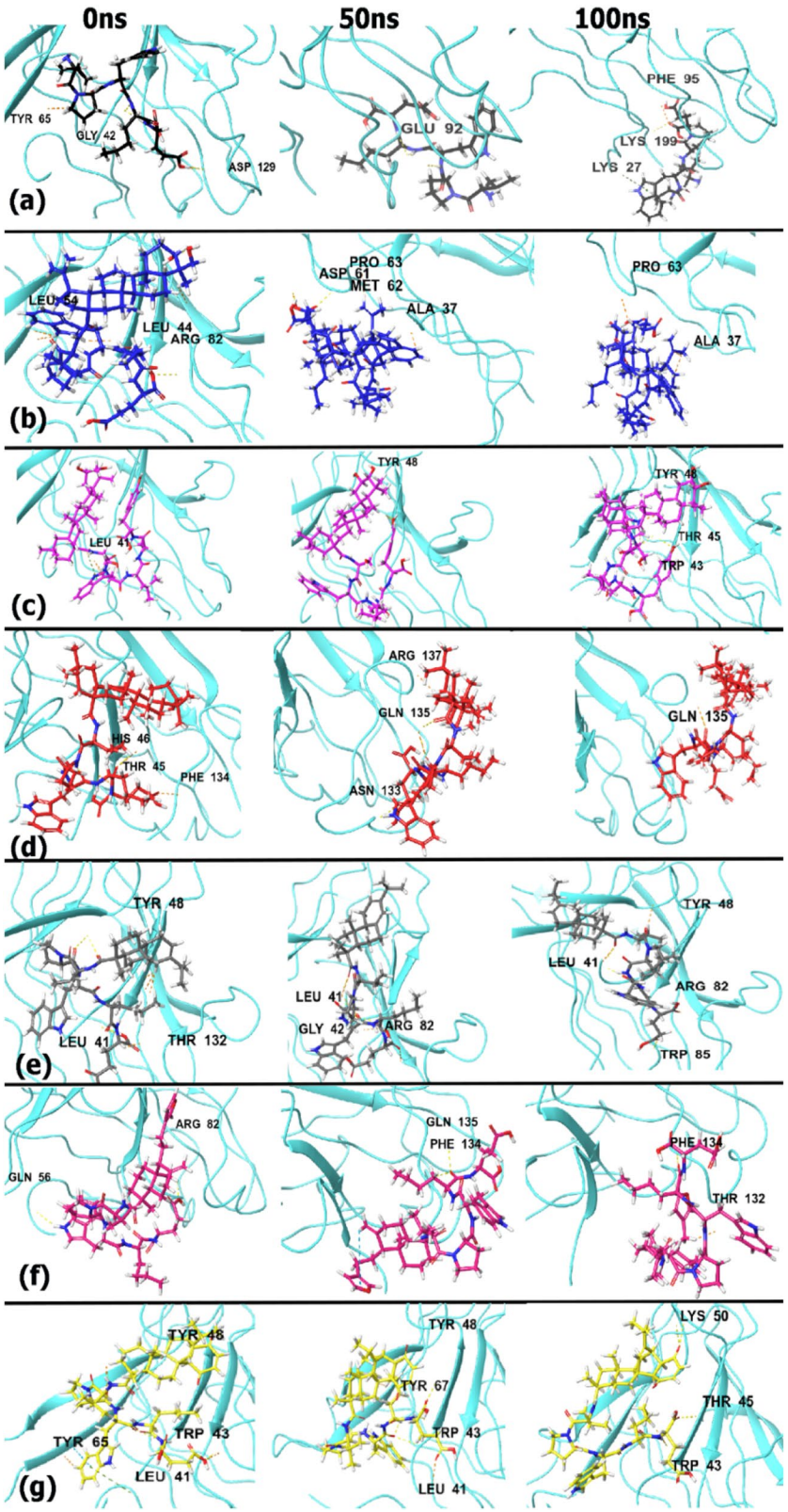

Fig. 8 Trajectory images of VPWXE and its conjugates with the ligand binding domain of EphA2 at 0 ns, 50 ns, and 100 ns of the simulation **a** VPWXE; **b** HB-amido-VPWXE; **c** MA-amido-VPWXE; **d** OA-amido-VPWXE; **e** LA-amido-VPWXE; **f** PA-amido-VPWXE; **g** QA-amido-VPWXE conjugate

Gln 136 and Tyr 122 in the beginning of the simulation and Gln 183 for the last 50 ns. However, binding interactions with Asn 120 is seen for the entire simulation. These new interactions in the presence of the linker confer a higher RMSD value however the difference is not significant. For the OA-amido-C4-VPWXE conjugate starts out very

Table 4 Average RMSD values obtained for terpene-linker-peptide receptor complex

Name of compound with Linker	Ligand binding domain of EphA2 receptor		Kinase domain of EphA2 receptor	
	P-L RMSD	Cα RMSD	P-L RMSD	Cα RMSD
MA-amido-C4-YSAYP	0.724	0.2406	0.7792	0.3263
OA-amido-C4-YSAYP	0.811	0.2765	0.6535	0.3331
MA-amido-C4-SWLAY	1.380	0.1987	0.5332	0.4024
OA-amido-C4-SWLAY	1.191	0.2490	0.5564	0.3123
MA-amido-C4-VPWXE	0.972	0.2545	0.5606	0.4200
OA-amido-C4-VPWXE	0.679	0.2039	0.6027	0.3440

well anchored to the receptor as seen by the low RMSD value until 37 ns. Throughout the simulation, it undergoes a change of conformation until the terpene region of the compounds becomes loose at the end of the simulation.

The kinase domain of EphA2 receptor also plays a critical role in several cellular processes and in the propagation of diseases. Studies have been conducted to elucidate the binding interactions of drug candidates with the EphA2 kinase binding domain in order to understand the differences and similarities with other RTKs implicated in cancer. To examine if the conjugates formed stable complexes with the kinase domain of the receptor, we carried out molecular dynamics studies. As can be seen in Table 3, across all of the conjugates, the average RMSD values were lower for the complexes with the kinase domain of the EphA2 receptor. This indicates that overall the conjugates may form more stable complexes with the EphA2 receptor kinase domain. This is likely because the EphA2 receptor kinase domain contains a larger hydrophobic pocket, that can bind to the conjugates more efficiently. In the case of the YSAYP conjugates, all conjugates showed lower RMSD values (< 1.0 nm). QA-amido-YSAYP conjugate had the lowest RMSD (0.36 nm) while the HB-amido YSAYP conjugate had a relatively higher value at 0.818 nm. All others were found to be in the range of 0.5 to 0.6 nm indicating high stability. The SWLAY conjugates also showed low RMSD values compared to those obtained with LBD. The lowest value was seen for the OA-amido-SWLAY conjugate at 0.38 nm. All other conjugates ranged from 0.5 to 0.69 nm, again implying the formation of more stable complexes with the EphA2 kinase domain. For the VPWXE conjugates also, we show lower average RMSD values (between 0.3 and 0.49 nm). These results indicate that the conjugates without the linker appear to have a higher affinity toward the EphA2 kinase domain.

After introducing the C4 linker (Table 4), the RMSD values for the linker conjugates with MA and OA were on average about similar or slightly higher compared to those obtained without the linker. The average RMSD values ranged from 0.55 to 0.77 nm in most cases. This suggests that while the incorporation of the linker did not significantly worsen the stability of the receptor ligand complex, it also did not enhance it (with exception of MA-amido-C4-SWLAY which showed slight reduction from 0.58 to 0.53 nm). To assess these results further, we explored the trajectories (Supplementary Information Fig. S5–S7). As can be seen, the YSAYP peptide interacts with residues within the DFG motif of the activation loop (Asp 757) and makes contacts with Lys 645 and Met 695 which are residues found within the hinge region of the ATP binding cleft. Over the course of the simulation, subtle changes are observed for the peptide within the cleft and while it continues to interact with Met 695, a new interaction is observed with Glu 693 toward the end of the simulation. For the conjugates, once again the hydroxybetulinic amido-YSAYP conjugate fits into the ATP binding cleft, and toward the end of the simulation the ligand also shows interactions with the C-helix region of the receptor. MA-amido-YSAYP also interacts with the G-rich region as well as the C-Helix and the activation loop, initially, however toward the end of the simulation, it makes critical contacts with Asp 757 of the DFG motif in the activation loop and moves away from the C-helix region. Hydrophobic contacts are observed with Ile 619 and the terpene moiety of the conjugate. For the OA-amido-YSAYP conjugate, Met 695 and Ile 619 appear to play a critical role in binding with the receptor, along with Glu 693. However, the ligand itself undergoes conformational change and folds up on itself by the end of the simulation. For the LA-amido-YSAYP conjugate, once again the ligand initially fits into the ATP binding cleft, and is spread out between the Gly-rich loop and the activation loop as well as with the C-helix making critical interactions, but by the end of the simulation, the ligand changes conformation and it moves away from the C-helix, though with a less extended conformation. For the PA-amido-YSAYP and QA-amido-YSAYP conjugates, interactions with Met 695, Tyr 694, and Ile 619 play role in hydrophobic interactions with the conjugate and appear to have strong interactions with the hinge region. The C-helix adopts an "in" conformation initially but midway through the simulation, it adopts an "out" conformation in the cases of QA and OA-amido-YSAYP conjugates. These results indicate that in all cases, binding interactions occurred within the ATP binding cleft for the peptide YSAYP and its terpene conjugates.

For SWLAY and its conjugates, interactions are observed with residues of the hinge region and Asp 757 of the activation loop. For SWLAY, the peptide undergoes conformation changes and toward the end of the simulation shows interaction with C-helix residue Glu 663 which hydrogen bonds with the –OH group of the terminal tyrosine of the peptide. For the HB-amido-SWLAY, initially the conjugate spans the entire ATP binding cleft, and is also seen interacting with one of the alpha helices of the C-lobe below the activation loop. However, toward the end of the simulation, the ligand moves upwards and makes hydrophobic contacts with Ile 619, Asp 659, and Val 627 in the hinge region. The MA-amido SWLAY and the OA-amido-SWLAY conjugates show similar interactions, encompassing the ATP binding cleft, with the terpene part of the conjugates interacting with the alpha-helices of the C-lobe, and the peptide portion with the activation loop making critical contacts with the DFG motif. In the case of the MA conjugate however, while the C-lobe interactions occur throughout the simulation, in the case of OA-amido-SWLAY conjugate, the terpene portion interacts with the residues of the C-helix. Additionally, the C-helix changes from an "in" conformation to "out" conformation in the case of the OA-amido SWLAY conjugate over the course of the simulation. In the case of the LA-amido SWLAY, the conjugate undergoes conformation changes throughout the simulation, though it maintains contact with the Asp 757 residue of the activation loop. The PA-amido-SWLAY conjugate makes initially interactions with the hinge region and the activation loop as well as the C-helix; however, by the end of the simulation, it moves toward the C-helix, while still maintaining contacts with the hinge region residues. The QA-amido SWLAY conjugate remains tethered to the activation loop throughout the simulation, though slight changes in conformation of the conjugate are observed, the main contacts with Met 695, Thr 692, Lys 646, and Ser 756 remain, thus accounting for its low RMSD and stability. One of the major differences observed between the SWLAY and the YSAYP conjugates was that several of the SWLAY conjugates interacted not only in the ATP binding cleft region but also with the C-lobe residues and the C-helix. This may be due to the presence of tryptophan residue, making it slightly more hydrophobic in the case of SWLAY.

The VPWXE peptide interacts with the hinge region and the gly-rich region, making contacts with residues such Lys 646, Asp 701, and Thr 692. The HB amido-VPWXE conjugate however occupies the entire ATP binding cleft, extending into the C-helix region. The MA and the OA-amido VPWXE conjugates remain tightly attached to the receptor kinase domain making contacts once again with the DFG motif residue Asp 757, alongside the gly-rich region residues Asp 659 and Lys 646. Additionally, interactions are also seen with the alpha-helices of the C-lobe. For the LA-amido-VPWXE however, the ligand undergoes major conformational changes and folds up during the course of the simulation, and interactions are observed with Ile 619 and Ala 621. The C-helix adopts an open conformation by the end of the simulation. Both QA and the PA-amido VPWXE conjugates also show changes in conformation over the course of the simulation, though primary contacts are seen with the hinge region. The QA-amido VPWXE conjugate almost moves out of the receptor, maintaining hydrophobic contacts with residues such as Ile 619 and Ala 621 with the peptide portion.

We then compared the trajectories of the MA and OA linker peptide conjugates (Supplementary Information Fig. S8). Similar to MA-amido-YSAYP, the corresponding linker incorporated conjugate retained the interaction with Glu 663 in the C-Helix throughout the entirety of the simulation. It also started out with interactions within the gatekeeper region as well as G-rich region. At the end of the simulation, the terminal tyrosine of the peptide was seen interacting with the gatekeeper residue. While the peptide chain portion experienced little fluctuations, the terpene region initially binds to Phe 758 of the DFG motif; however, at the end, it fails to anchor itself to the receptor. This supports the slightly increased RMSD value that was seen for the linker. The OA-amido-C4-YSAYP conjugate retained the interaction with Met 695 that was determined to play a critical role in binding the OA-amido-YSAYP to the receptor. In fact, even though other interactions take place throughout the simulation, at the end of the simulation Met 695 is crucial in keeping the linker-incorporated conjugate anchored to the receptor through an interaction with the terminal –OH group of the terpene group. For the MA-amido-C4-SWLAY, binding occurs in the same region throughout the simulation, namely in the DFG motif, ribose pocket, hinge region, and ATP binding pocket entrance. The terpene portion of the conjugate fluctuated the most; however, it is able to remain anchored to the receptor unlike in the case of the conjugate without the linker, which justifies why its RMSD value was slightly lower, representing higher stability of the receptor ligand complex. The OA-amido-C4-SWLAY also retained many of the interactions that were present for the corresponding non-linker conjugate, namely Lys 646, Glu 663, and Asp 757. Similarly, the MA-amido-C4-VPWXE and the OA-amido-C4-VPWXE conjugates also remained tightly bound, making contacts in similar regions as their respective non-containing linkers such as interactions with the DFG motif and Gly-rich loop.

Overall, these results indicate that several of the conjugates had stronger interactions with the tyrosine kinase domain of the EphA2 receptor compared to the ligand binding domain and may be considered for further studies for designing drugs for targeting cancer. Incorporation of the linker resulted in comparatively stronger interactions with

the LBD region, while it slightly reduced interactions with the EphA2 kinase domain. The trajectories of the terpenes showed significantly lower binding though the terpenes also attached to the EphA2 kinase binding domain (Supporting Information Fig. S9) making key contacts with residues such as Met 695 and Asp 757. Previous work has also shown that plant terpenes such as oleanolic acid and urosolic acid may play a key role in reducing cell proliferation of tumor cells by inhibiting tyrosine kinases [82, 83].

We next compared the RMSF values which provide us with the information regarding the flexibility of the protein upon interacting with a ligand [84]. The results are shown in Fig. 9. As can be seen in the figure, in the case of the LBD of the receptor, all conjugates as well as the peptide alone resulted in higher flexibilities in the same regions of the protein though the RMSF values varied depending upon the conjugates. The residues involved included Ala 37, Lys 50, Asn 60, Gly 75, Gly 100, and Val 161. This indicates that the conjugates were likely binding mostly in the G-H loop regions along with some interactions in the J-K loop as well as the D-E region in some cases. The unbound peptides showed relatively lower flexibilities.

When compared with the neat terpenes (Fig. 9g), it was observed that the same amino acid residues contribute to the movement of the protein during the simulation. The same pattern in seen for the MA and OA conjugates containing the linkers where RMSF values range similar to the values of the conjugates without the linkers as seen in Supplementary Information Fig. S10b. For the LBD, highest flexibility was seen for the residues including Asp 33, Asn 57, and Phe 108 indicative of higher motion of the receptor in this region. Interestingly, the MA-amido-C4-VPWXE showed higher flexibility compared to the other conjugates in the Val 161

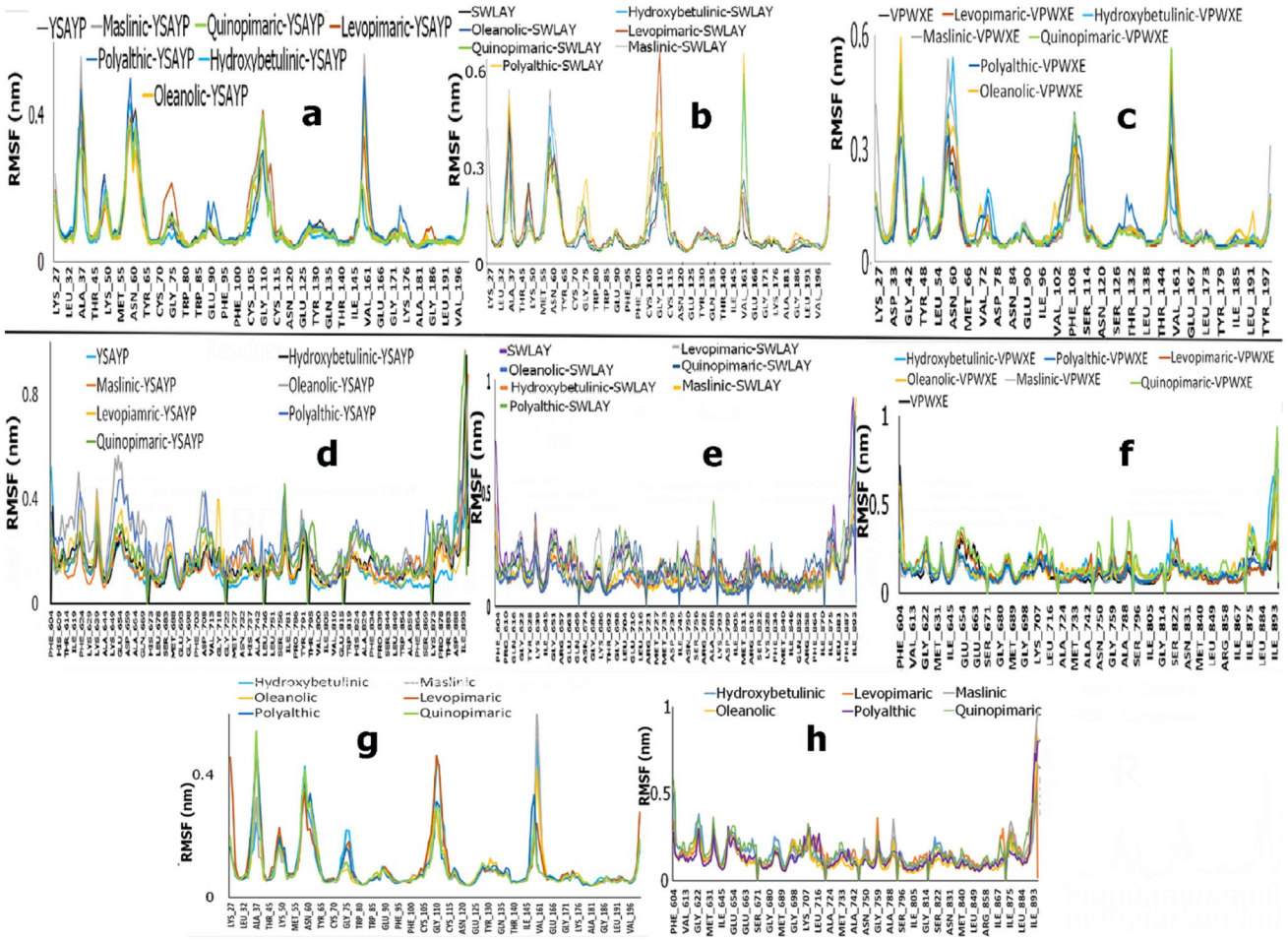

Fig. 9 Comparison of protein RMSFs of **a** YSAYP and its terpene conjugates with the LBD of EphA2; **b** SWLAY and its terpene conjugates with the LBD of EphA2; **c** VPWXE and its terpene conjugates with the LBD of EphA2; **d** YSAYP and its terpene conjugates with the kinase binding domain of EphA2; **e** SWLAY and its terpene conjugates with the kinase binding domain of EphA2; **f** VPWXE and its terpene conjugates with the kinase binding domain of EphA2 receptor; **g** Neat terpenes with the LBD of EphA2; and **h** Neat terpenes with the kinase binding domain of EphA2 receptor

region, whereas MA-amido-C4-YSAYP showed higher flexibility in the region between Asn 57 and Pro-63.

In the case of the kinase domain, relatively lower fluctuations compared to the ligand binding domain was observed. Among the conjugate receptor complexes, relatively higher fluctuations were observed for the YSAYP conjugates, while the SWLAY and the VPWXE conjugates showed lower fluctuations. In all cases, the C-terminal residues showed high fluctuations, which is due to higher flexibility [85]. The residues showing fluctuations were interestingly different for each ligand complexed with the kinase domain. For the YSAYP peptide and its conjugates, residues Ile 619, Lys 649, Glu 656, Asp 708, Ile 781Tyr 791, and His 824 showed fluctuations while the OA-amido YSAYP conjugate showing highest fluctuations with Glu 654 and Lys 649. In the case of the SWLAY conjugates, all conjugates showed approximately similar fluctuations, with residues Tyr 628, Gly 651, Leu 704, Leu 710, Ala 788, Met 840, and Ile 875. Thus hydrophobic interactions played a large role in stabilizing the SWLAY-conjugate complexes. The values for the VPWXE complexes also showed relatively low RMSF values (< 0.5 nm), with the QA conjugate showing slightly higher fluctuations. Residues involved included Gly 622, Glu 654, Leu 716, Gly 759, Ser 796, and Ser 822, indicating more H-bonding interactions being involved in stabilizing this complex. For the kinase domain with terpenes alone, residues that showed higher flexibility included Gly 622, Met 631, Glu 634, Gly 759, and Ala 788 indicating that some of the residues include those in the gly-rich loop as well as the catalytic region. For the MA and OA conjugates with the linker (Supplementary Information Fig. S10a), the highest flexibility was seen in the C-terminal region which is expected given that the terminal residues are expected to be flexible. Other regions that showed relatively higher flexibility for most conjugates were Val 658, Lys 655, Glu 706, Ala 699, Leu 746, and Met 827. Relatively higher flexibility was seen for the MA-amido-C4-SWLAY conjugate, particularly in the region of Met 733. The olealonate-amido-C4-SWLAY conjugate showed relatively higher flexibility in the Val 658 region. These results indicate that overall, the linker conjugates were interacting more with the hydrophobic residues of the EphA2 kinase binding domain.

ADME studies

For further analysis of the designed conjugates, we examined their properties using the web server ADMETlab2.0. Results of log P values for each of the conjugates and individual terpenes are shown in Table 5. In general, log P is the partition coefficient between the lipophilic phase and aqueous phase and provides critical information regarding the absorption and distribution of the pharmacological candidate [86]. All the conjugates as well as the unconjugated peptides and the neat terpenes were studied. The neat terpenoids had a high log P values ranging from 4.292 to 6.645 due to their hydrophobicity. In comparison, the neat peptides had a much lower logP values, as they were less hydrophobic. Upon conjugation with the terpenes, there was an increase in logP value compared to the YSAYP peptide, as expected. The highest logP value was seen for the OA-amido-YSAYP as was expected and also predicted from COSMO-RS studies discussed earlier. Similarly, upon conjugating the terpenes with the SWLAY peptide as well as the VPWXE peptide, there was also an increase in logP value. Overall, the VPWXE conjugated peptides had the highest logP value compared to the conjugates with the other peptides as was expected since the VPWXE peptide was the most hydrophobic of the three peptides. These

Table 5 ADME studies

Compound	LogP
Hydroxybetulinic acid	4.582
Maslinic Acid	5.798
Oleanolic acid	6.645
Levopimaric acid	4.292
Polyalthic acid	4.685
Quinopimaric acid	4.558
YSAYP	-1.435
HB-amido-YSAYP	4.264
MA-amido-YSAYP	5.626
OA-amido-YSAYP	6.328
LA-amido-YSAYP	3.869
PA-amido-YSAYP	3.784
QA-amido-YSAYP	4.355
MA-amido-C4-YSAYP	5.22
OA-amido-C4-YSAYP	6.022
SWLAY	0.48
HB-amido-SWLAY	5.142
MA-amido-SWLAY	5.19
OA-amido-SWLAY	7.357
LA-amido-SWLAY	5.272
PA-amido-SWLAY	5.384
QA-amido-SWLAY	5.873
MA-amido-C4-SWLAY	6.490
OA-amido-C4-SWLAY	7.181
VPWXE	0.544
HB-amido-VPWXE	5.819
MA-amido-VPWXE	7.081
OA-amido-VPWXE	7.67
LA-amido-VPWXE	5.557
PA-amido-VPWXE	6.369
QA-amido-VPWXE	6.134
MA-amido-C4-VPWXE	6.583
OA-amido-C4-VPWXE	7.481

results indicate that some of the peptide conjugates displayed drug-like properties and may be utilized for further development for targeting tumors. For the MA and OA peptide conjugates with the C4 linker, as expected the logP values further increased due to incorporation of the C4 aliphatic linker.

Cell viability studies

Given the promising results of the conjugates using computational methods, we chose to explore in vitro cellular interactions with undifferentiated glioma F98 cells which are known to overexpress EphA2 receptor [87, 88]. This cell line has been developed for numerous studies for developing tumor models for glioblastoma multiforme [89]. We also examined interactions with human fibroblasts, to study the viability of non-cancer cell lines in the presence of the conjugates. As a proof of concept, we synthesized MA and OA conjugates with YSAYP, SWLAY, and VPWXE peptides by standard coupling methods where the carboxyl group of the terpenes was conjugated with the N-terminal of each peptide.

Cell viability studies were then carried out and results are shown in Fig. 10. As seen in Fig. 10a, the neat peptides SWLAY and YSAYP showed minimal effect on the proliferation of F98 cells and cells treated with those peptides were found to have an overall viability of approximately on average 85–88%. In case of neat VPWXE however, a slight decrease in viability was observed at 82%. In previous studies, the VPWXE motif has been shown to have a high specificity toward tumor cells [90] and it is likely that the VPWXE may have an effect in reducing viability, particularly at higher concentrations. For the conjugates, results indicate that MA-amido-YSAYP resulted in a slight decrease in viability of the F98 cells (~75%), although the cells continued to proliferate. For the OA-amido YSAYP conjugate however, a significant decrease in viability was observed,

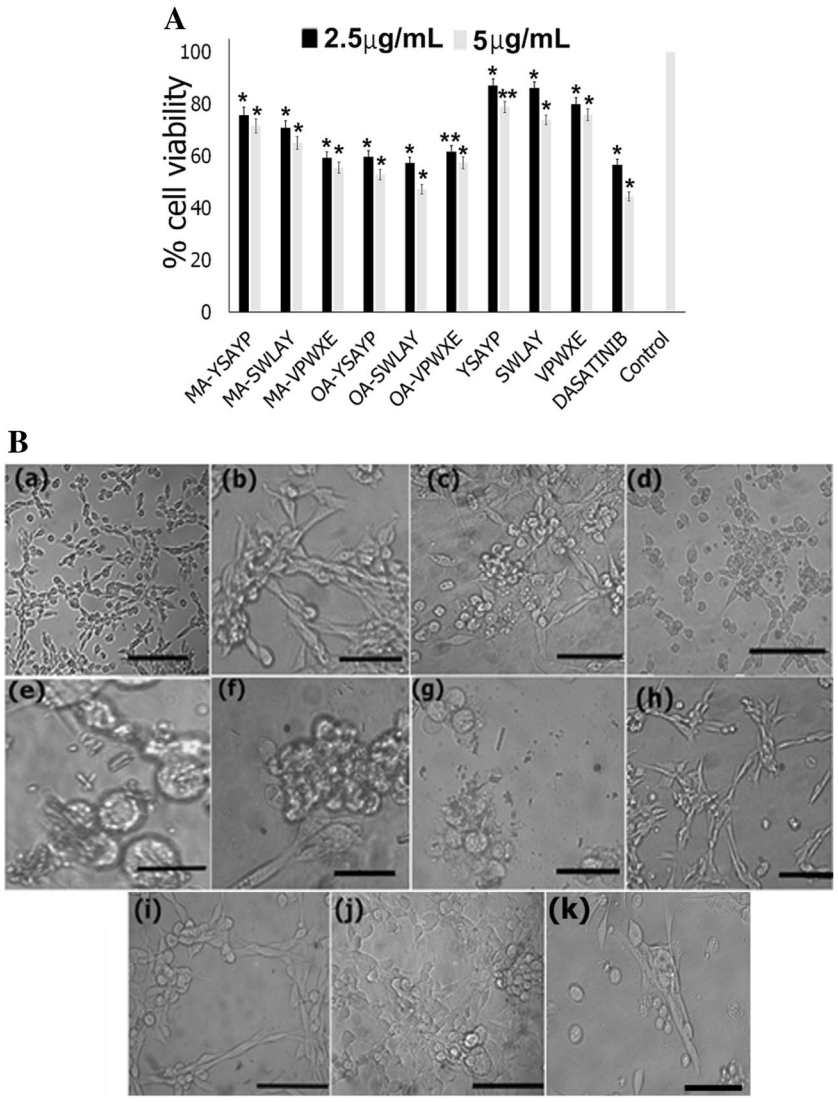

Fig. 10 **A**. Cell viability studies of F98 cells in the presence of varying concentrations of MA and OA-amido conjugates, Dasatinib, as well as the neat peptides YSAYP; SWLAY and VPWXE. (*$P < 0.05$; **$P < 0.01$). (Statistical Analysis was carried out using Students *t* test). **B**. Optical microscopy images of cells after 24 hours of incubation with constructs (**a**) Control cells; (**b**) cells treated with MA-amido-YSAYP; (**c**) cells treated with MA-amido-SWLAY; (**d**) MA-amido-VPWXE; (**e**) cells treated with OA-amido-YSAYP; (**f**) cells treated with OA-amido-SWLAY; (**g**) cells treated with OA-amido-VPWXE; (**h**) cells treated with SWLAY; (**i**) cells treated with YSAYP; (**j**) cells treated with VPWXE (**k**) cells treated with Dasatinib

particularly at the higher concentration (52% viability) thus signifying that the OA-moiety plays a role in reduction of F98 cell viability. This corroborates with previous results that have shown that oleanolic acid has tumor-suppressive effects and reduces cell migration in glioma cells by inhibiting the MAPK-/ERK pathway [91]. Furthermore, it has also been shown to reduce proliferation in varying cancer cell lines such as MCF-7 and HT-29 [92, 93] by inducing apoptosis through G2/M phase cell cycle arrest. Among the SWLAY conjugates, once again OA-amido-SWLAY conjugate showed higher cytotoxicity (57% viability at lower concentration and 47% at the higher concentration), compared to the MA counterpart. Though MA conjugated with SWLAY did inhibit proliferation (70% viability at the lower concentration). The cytotoxicity of the VPWXE conjugates was found to be concentration dependent with oleanolate-amido-VPWXE showing similar cytotoxicity as the MA counterpart (61% and 59% respectively at the lower concentration and 55% at the higher concentration for both). In general, compared to the peptides alone, the conjugates displayed higher cytotoxicity thus implying that conjugation with terpenes increases cytotoxicity toward tumor cells. The positive control (Dasatinib) showed a reduction in cell proliferation to 44% at the higher concentration, which is comparable to that observed for oleanolate-amido-SWLAY at 47%. To further confirm these results, we examined the morphologies of the cells after treatment with the conjugates and peptides for 24 h at 5 µg/mL concentration of each conjugate/peptide. As can be seen in Fig. 10b, the MA conjugates appear to look similar to the control cells and displayed widespread extensions making several contacts with cells signifying mostly healthy cells. However, in the case of the OA conjugates, fewer extensions were observed and cells appeared rounded. This indicates that their growth was slowed down as this type of morphology is generally seen in the initial stages of growth of glioma cells [94] and that cell proliferation was being stunted. In the presence of the peptides however, once again the cells appear well spread, and making contacts with adjacent cells. With the VPWXE, some aggregation of rounded cells is also observed. In the presence of the drug Dastanib, overall, while there were some cells that appeared to form extensions, a significant amount of cells were also found to round up. Overall, these results agree with the WST-8 viability studies.

To further investigate the effects on non-cancer cell lines, we examined the effects on human dermal fibroblasts, and the results obtained are shown in Supplementary Information Fig. S11. As can be seen, upon treatment with all conjugates, the cells continued to proliferate and had a viability greater than 92%. The cells also formed typical elongated shapes signifying healthy cells. These results indicate that the conjugates (particularly the OA-amido-YSAYP and OA-amido-SWLAY peptide conjugates) had specificity toward the F98 glioma cells.

Apoptosis studies

In order to elucidate the mechanism, an apoptosis assay was performed, and the results can be seen in Fig. 11. As can be seen in the figure, at 24 h, in the presence of OA-amido-SWLAY (Fig. 11a) and OA-amido-YSAYP (Fig. 11b), the treated glioma cells appear to be intracellularly stained with the red propidium iodide dye. This is supported by the fact that we see extensive blebbing and disrupted membrane [95, 96] indicative of late-apoptosis. In contrast, OA-amido-VPWXE (Fig. 11c) was stained green indicating that it induces apoptosis that is only at its early stages. This is confirmed by the circular green fluorescence that is seen around the cells which is due to annexin V binding to the exposed phosphatidylserine on the membrane of the cell rather than intracellularly as well as the fact that the integrity of the membrane has not been compromised [97]. Additionally, VPWXE and MA-amido-SWLAY also induced early apoptosis, while MA-amido-VPWXE showed late apoptotic cells. No apoptosis was observed in the

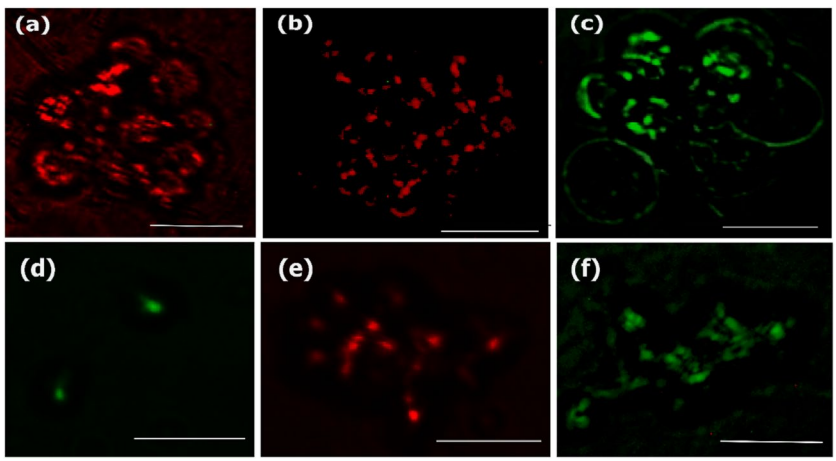

Fig. 11 *Apo*ptosis assay carried out after 24 h of incubation of various conjugates with F98 cells. **a** OA-amido-SWLAY conjugate; **b** OA-amido-YSAYP; **c** OA-amido-VPWXE; **d** VPWXE; **e** MA-amido-VPWXE; **f** MA-amido-SWLAY. Scale bar = 25 µm

case of the SWLAY or YSAYP individually. These results indicate that conjugating the peptides (particularly SWLAY) with these specific terpenes promotes apoptosis of F98 cells. This corroborates with previous work, where it has been shown that both MA and OA terpenes induce apoptosis in tumor cells [98, 99]. However, the signaling pathways induced by these conjugates on F98 cells needs to be further studied, in the context of binding interactions with the EphA2 receptors. Those studies are currently ongoing and will be reported separately.

ADP-Glo assay

Given that MA and OA peptide conjugates showed promising results with F98 cells, we further selected these conjugates to test if EphA2 kinase enzyme inhibition was involved. We therefore determined the kinase activity in the presence and absence of the conjugates using ADP-Glo kinase assay which is a well-known method, and is utilized to examine kinase activity by quantifying the amount of ADP produced during kinase reactions [100]. For the control reaction, DMSO vehicle control was used, keeping all other conditions the same. Results obtained are shown in Fig. 12. As shown in the figure, we observed that the highest inhibitory activity was observed for the OA-amido-SWLAY conjugate (49.4% inhibition) at 30 µM concentration, while almost no inhibitory effect was seen for the MA-amido-VPWXE conjugate (10.2% inhibition) at the same concentration.

The MA-amido-SWLAY conjugate displayed 38.3% inhibition, while MA-amido-YSAYP showed 32% inhibition at the same concentration. The OA-amido-YSAYP conjugate was comparable to the MA counterpart showing 33% at the same concentration. Interestingly, the oleanolate-amido-VPWXE conjugate did show some inhibition, though less than the others at 25% at the same concentration. Overall, the SWLAY conjugates showed slightly higher inhibition of EphA2 kinase activity compared to the YSYAP conjugates. These results indicate that the oleanolate and Maslinate SWLAY and YSAYP conjugates do display kinase inhibition activity at higher concentrations of the conjugates utilized in this study, though the SWLAY conjugates showed higher potency.

SPR analysis

To further determine the specificity of binding interactions of the EphA2 receptor with the peptide conjugates, we carried out SPR analysis at varying concentrations with both the kinase-binding domain and the ligand-binding domain of the receptor. Results obtained are shown in Table 6. Because oleanolate-amido-SWLAY showed the most promising results with cells as well as with the ADP-Glo assay, as a proof of concept, we carried out SPR analysis with the oleanolate-amido-SWLAY conjugate. Additionally,

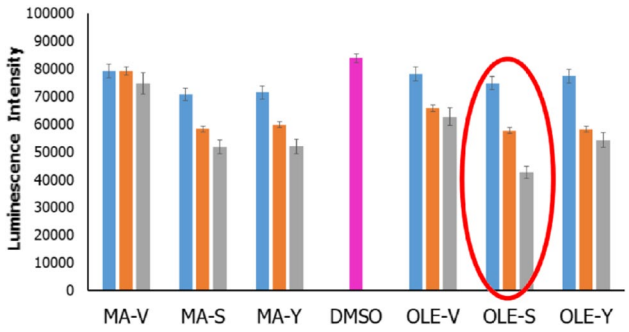

Fig. 12 EphA2 kinase activity in the presence of peptide conjugates of MA and OA. All reactions were done in the presence of substrate. DMSO was used as the vehicle control. The average values of n = 3 and standard deviation are shown. S, Y, and V are abbreviations for SWLAY, YSAYP, and VPWXE. Ole = olealonate; MA = Maslinate. The concentrations of the conjugates are blue = 10 µM; orange = 20 µM and grey = 30 µM. The substrate concentration was kept constant at 20 µM. Ole-S is circled in red indicating highest inhibitory activity

Table 6 Binding affinity (KD) using SPR analysis

Test compound	KD (M)	Domain
OA Amido-SWLAY	0.377e-006	Kinase-binding domain
Dasatnib (positive control)	5.411e-007	Kinase-binding domain
Ephrin A1 (positive control)	0.8134e-006	Ligand-binding domain
OA Amido-SWLAY	0.7393e-003	Ligand-binding domain

the drug Dasatinib was studied as a positive control for the kinase-binding domain as it is a well-known kinase inhibitor and binds efficiently to the kinase domain of receptors [101]. Similarly, EphA1 protein which is the natural ligand for ligand binding domain of the receptor was also studied as a positive control for the ligand-binding domain. As can be from the results, for the oleanolate-amido-SWLAY a higher binding (lower KD) was observed for the kinase domain compared to the ligand-binding domain. Though there was slight binding, the KD was higher for the ligand-binding domain compared to the natural ligand EphA1. Such minor binding is expected, given that the SWLAY peptide by itself is known to bind to the ligand-binding domain as discussed earlier.

These results also validate the computational studies which indicated increased binding interactions between the kinase domain and the oleanolate-amido-SWLAY compared to SWLAY alone. As expected, Dasatinib showed high binding with the kinase domain. The value obtained for the Dasatinib is comparable to previous values obtained from other studies [102]. The KD value obtained for the oleanolate-amido-SWLAY was comparable, further validating its interactions with the kinase binding domain of the receptor.

Conclusions

In this work, we have explored the interactions of newly designed peptide conjugates of six naturally occurring terpenes with both the EphA2 kinase domain and ligand-binding domain of the EphA2 receptor. Two peptides that were previously shown to recognize and bind to the ligand binding domain of the receptor were chosen, namely SWLAY and YSAYP. We also selected a known RTK-binding peptide (VPWXE) as a control to examine specificity. Molecular dynamics and docking studies conducted indicated that most of the conjugates had a higher binding affinity and formed stable complexes with the EphA2 kinase domain of the receptor compared to the ligand-binding domain. Furthermore, many of the conjugates were found to firmly attach to the ATP binding pocket making contacts with critical residues in the hinge region and the activation loop. The ligand-binding domain, however, showed the formation of relatively less stable complexes, particularly when the terpenes were conjugated to the YSAYP peptide due to the highly flexible nature of the ligand-binding domain. More stable complexes were observed with the SWLAY conjugates. Conjugation with VPWXE yielded the least stable complexes with the ligand-binding domain. We also conducted computational studies where in a linker (C4 aliphatic chain) was incorporated into the conjugates. Results showed that the linker conjugates enhanced interactions and formed more stable complexes with the ligand-binding domain, while interactions with EphA2 kinase-binding domain were about the same or slightly lower upon incorporation of the linker. ADME studies also showed increase in logP values upon incorporation of the linker. Based on the computational results obtained, we selected two terpenes (OA and MA) and conjugated those with all three peptides and examined their efficacy against F98 glioma tumor cells. Our results showed that conjugation with the terpenes reduced the viability of the cells. In particular, OA conjugates resulted in a higher cytotoxicity toward the tumor cells, thus indicating those conjugates may be developed for specifically targeting tumor cells. Mechanistically, the cells appeared to undergo apoptosis. Finally, ADP-glo assay studies revealed that the OA-amido-SWLAY and potentially MA-amido-SWLAY conjugate may also function as EphA2 kinase inhibitors at higher concentrations. SPR analysis with the OA-amido-SWLAY conjugate also confirmed binding with the receptor with a higher affinity toward the kinase domain. Thus, we have developed a new family of terpene linked-short-peptide conjugates that may be potentially developed to target tumor cells, particularly those over-expressing the EphA2 receptor. Further studies on the linker conjugates can be interesting and will be explored in a future study.

Supplementary Information The online version contains supplementary material available at https://doi.org/10.1007/s00894-023-05596-3.

Acknowledgements BG thanks the Clare Boothe Luce Foundation and Fordham University Research Grant for financial support of this work. BG also would like to thank Ms. Lucy Hart for her assistance with cell studies. IB thanks Fordham University research grants for financial support of this work.

Author contribution Ipsita Banerjee was responsible for conception and design. Material preparation and data collection was performed by Beatriz Goncalves. The first draft of the manuscript was written by Beatriz Goncalves and both authors commented on previous versions of the manuscript. Beatriz Goncalves and Ipsita Banerjee were responsible for data analysis. Final manuscript was written and edited by Ipsita Banerjee.

Funding Fordham University Research Grants.

Data availability Additional data available in supporting documents, and manuscript will be available on the faculty website.

Declarations

Competing interests The authors declare no competing interests.

References

1. Farnsworth NR, Akerele O, Bingel AS, Soejarto DD, Guo Z (1985) Medicinal plants in therapy. Bull World Health Org 63:965–981
2. Yusof Y (2016) Gingerol and Its Role in Chronic Diseases. Adv Exp Med Biol 929:177–207
3. Kytidou K, Artola M, Overkleeft HS, Aerts JMFG (2020) Plant glycosides and glycosidases: a treasure-trove for therapeutics. Front Plant Sci 11:357
4. Karim N, Khan H, Khan I, Guo O, Sobarzo-Sanchez E, Rastrelli L, Kamal MA (2020) An increasing role of polyphenols as novel therapeutics for Alzheimer's: a review. Med Chem 16:1007–1021
5. Kohli SK, Bhardwaj A, Bhardwaj V, Sharma A, Kalia N, Landi M, Bhardwaj R (2020) Therapeutic potential of brassinosteroids in biomedical and clinical research. Biomolecules 10:572
6. Lu J-J, Dang Y-Y, Huang M, Xu W-S, Chen X-P, Wang Y-T (2012) Anti-cancer properties of terpenoids isolated from rhizoma curcumae-A review. J. Ethnopharmacol. 143:406–411
7. Rarova L, Zahler S, Liebl J, Krystof V, Delka D, Bartunek P, Kohout L, Strnad M (2012) Brassinosteroids inhibit in vitro angiogenesis in human endothelial cells. Steroids 77:1502–1509
8. Yang SS, Cragg GM, Newman DJ (2001) The Camptothecin experience: from Chinese medicinal plants to potent anti-cancer drugs. Drug Discov Tradition Chin Med 61:74
9. Khazir J, Mir BA, Pilcher L, Riley DL (2014) Role of plants in anticancer drug discovery. Phytochem Lett 7:173–181
10. Zhang QT, Liu ZD, Wang Z, Wang T, Wang N, Zhang B, Zhao Y-F (2015) Recent advances in small peptides of marine origin in cancer therapy. Mar Drugs 19:115
11. Pachebafi A, Tamanaee F, Ehteram H, Ahmad E, Niksad H, Kashani H (2022) The dual interaction of antimicrobial peptides on bacteria and cancer cells; mechanism of action and therapeutic strategies of nanostructures. Microb Cell Fact 21:1–18
12. Kim Y, Lillo AM, Steiniger SC, Liu Y, Ballatore C, Anichini A, Mortarini R, Kaufmann GF, Zhou B, Felding-Habermann B, Janda KD (2006) Targeting heat shock proteins on cancer

cells: selection, characterization and cell-penetrating properties of GRP78 ligand. Biochemistry 45:9434–9444
13. Alves DS, Westerfield JM, Shi X, Nguyen VP, Stefanski KM, Booth KR, Kim S, Morrell-Falvey J, Wang B-C, Abel SM, Smith AW, Barrera FN (2018) A novel pH-dependent membrane peptide that binds to EphA2 and inhibits cell migration. eLife 7:336645
14. Miao H, Li D-Q, Mukherjee A, Guo H, Petty A, Cutter J, Basilion JP, Sedor J, Wu J, Danielpour D, Sloan AE, Cohen ML, Wang B (2009) EphA2 mediates ligand-dependent inhibition and ligand-independent promotion of cell migration and invasion via reciprocal regulatory loop with Akt. Cancer Cell 16:9–20
15. Renee CI, Jin C (2005) EphA2 receptor tyrosine kinase as a promising target for cancer therapeutics. Curr Cancer Drug Targets 5:149–157
16. Brannan JM, Dong W, Prudkin L, Behrens C, Lotan R, Bekele BN, Wistuba I, Johnson FM (2009) Expression of the receptor tyrosine kinase EphA2 is increased in smokers and predicts poor survival in non-small cell lung cancer. Clin Cancer Res 15:4423–4430
17. Miao H, Wei BR, Peehl DM, Li Q, Alexandrou T, Schelling JR, Rhim JS, Sedor JR, Burnett E, Wang B (2001) Activation of EphA receptor tyrosine kinase inhibits the Ras/MAPK pathway. Nat Cell Biol 3:527–530
18. Yang NY, Fernandez C, Richter M, Xiao Z, Valencia F, Tice DA, Pasquale EB (2011) Crosstalk of the EphA2 receptor with a serine/threonine phosphatase suppresses the Akt-mTORC1 pathway in cancer cells. Cell Signal 23:201–212
19. Taddei ML, Parri M, Angelucci A, Onnis B, Bianchini F, Giannoni E, Raugei G, Calorini L, Rucci N, Teti A, Bologna M, Chiarugi P (2009) Kinase-dependent and independent roles of EphA2 in the regulation of prostate cancer invasion and metastasis. Am J Pathol 174:1492–1503
20. Pasquale EB (2005) Eph receptor signaling casts a wide net on cell behavior. Nat Rev Mol Cell Biol 6:462–475
21. Wu B, Wang S, De SK, Barile E, Quinn BA, Zharkikh I, Purves A, Stebbins JL, Oshima RG, Fisher PB, Pellecchia M (2015) Design and characterization of novel EphA2 agonists for targeted delivery of chemotherapy to cancer cells. Chem Biol 22:876–887
22. Blackburn WH, Dickerson EB, Smith MH, McDonald JF, Lyon LA (2009) Peptide-functionalized nanogels for targeted siRNA delivery. Bioconjug Chem 20:960–968
23. Dickerson EB, Blackburn WH, Smith MH, Kapa LB, Lyon LA, McDonald JF (2010) Chemosensitization of cancer cells by siRNA using targeted nanogel delivery. BMC Cancer 10:10
24. Singh DR, Pasquale EB, Hristova K (2016) A small peptide promotes EphA2 kinase-dependent signaling by stabilizing EphA2 dimers. Biochim Biophys Acta 1860:1922–1928
25. Lectenberg BC, Gehring MP, Light TP, Horne CR, Matsumoto MW, Hristova K, Pasquale EB (2021) Regulation of EphA2 receptor intracellular region by phosphomimetic negative charges in the kinase-SAM linker. Nature Commun 12:7047
26. Purba ER, Saita EI, Maruyama IN (2017) Activation of the EGF receptor by ligand binding and oncogenic mutations: The rotation model. Cells 6:13
27. Mitra S, Duggineni S, Koolpe M, Zhu X, Huang Z, Pasquale EB (2010) Structure-activity relationship analysis of peptides targeting the EphA2 receptor. Biochemistry 49:6687–6695
28. Tognolini M, Incerti M, Pala D, Russo S, Castelli R, Hassan-Mohamed I, Girogio C, Lodola A (2014) Target hopping as a useful tool for the identification of novel EphA2 protein-protein antagonists. Chem Med Chem Commun 9:67–72
29. Giorgio C, Hassan-Mohamed I, Flammini L, Barocelli E, Incerti M, Lodola A, Tognolini M (2011) Lithocholic acid is an Eph-Ephrin ligand interfering with Eph-kinase activation. PLoS ONE 6:e18128
30. Seigler DS (1998) Triterpenes and steroids (Chapter 23). In: Plant secondary metabolism. Springer, Boston pp 427–455. https://doi.org/10.1007/978-1-4615-4913-0_23
31. Incerti M, Tognolini M, Russo S, Pala D, Giorgio C, Hassan-Mohamed I, Noberini R, Pasquale EB, Vicini P, Piersanti S, Rivara S, Barocelli E, Mor M, Lodola A (2013) Amino acid conjugates of lithocholic acid as antagonists of the EphA2 receptor. J Med Chem 56:2936–2947
32. Yang ML, Teck YW, Hsum YW, Hoon LS, Chieng YC (2012) Suppressive effect of MA acid on PMA-induced protein kinase C in human lymphoblastoid cells. Asian Pacific J. Cancer Prevent 13:1513–7368
33. Murata S, Sasaki T, Yamauchi Y, Shimizu M, Ryuichiro S (2021) MA acid activates mTORC1 and human TGR5 and induces skeletal muscle hypertrophy. Biosci Biotechnol Biochem 85:2311–2321
34. Ganatra SH, Suchak AS (2012) Studies of Naturally Occurring Terpene based Compounds with Cyclin-Dependent Kinase 2 Enzyme. J Comput Sci Syst Biol 5:2
35. Flekhter OB, Tretyakova EV, Makara NS, Gabdrakhmanova SF, Baschenko BZ, Galin FZ, Zarudii FS, Tolstikov GA (2003) Search for new drugs. Pharm Chem J 37:142–144
36. Zhang K, Ding J (2020) In vitro anticancer effects of levopimaric acid in cisplatin-resistant human lung carcinoma are mediated via autophagy, ROS-mediated mitochondrial dysfunction, cell apoptosis and modulation of ERK/MAPK/ JNK signaling pathway. J Buon 25:248–254
37. Yu L, Xie X, Cao X, Chen J, Chen G, Chen Y, Li G, Qin J, Peng F, Peng C (2021) The anticancer potential of MA acid and its derivatives: a review. Drug Des Devel Ther 15:3863–3879
38. Duan L, Yang Z, Jiang X, Zhang J, Guo X (2019) Oleanolic acid inhibits cell proliferation migration and invasion and induces SW579 thyroid cancer cell line apoptosis by targeting forkhead transcription factor A. Anticancer Drugs 8:812–820
39. Hossein-Nejad-Ariani H, Althagafi E, Kaur K (2019) Small peptide ligands for targeting EGFR in triple negative breast cancer cells. Sci Rep 9:2723
40. Schrödinger L, DeLano W (2020) PyMOL. Available from: http://www.pymol.org/pymol. Accessed Feb 2023
41. Balasubramani SG, Chen GP, Coriani S, Diedenhofen M, Frank MS, Franzke YJ, Furche F, Grotjahn R, Harding M, Hattig C, Hellweg A, Helmich-Paris B, Holzer C, Huniar U, Kaupp M, Hhah AM, Khani SK, Muller T, Mack F, Nguyen B, Parker SM, Perit E, Rappoport D, Reiter K, Roy S, Rukcert M, Schmitz G, Sierka M, Tapavicza E, Tew DP, van Wullen C, Voora V, Weigend F, Wodynski A, Yu J (2020) Turbomole: modular program suite for ab initio quantum-chemical and condensed matter simulations. J Chem Phys 152:184107
42. Mullins E, Oldland R, Liu YA, Wang S, Sandler SI, Chen C, Zwolak M, Seavey KC (2006) Sigma-profile database for using COSMO-based thermodynamic methods. Ind Eng Chem Res 45:4389–4415
43. Miquel M, Massel M, DeSilva A, Palomar J, Rodriguez F, Brennecke JF (2014) Excess enthalpy of monoethanolamine + ionic liquid mixtures: how good are COSMO-RS predictions? J Phys Chem B 118:11512–11522
44. Simões T, Lopes D, Dias S, Fernandes F, Pereira J, Jorge J, Bajaj C, Gomes A (2017) Geometric detection algorithms for cavities on protein surfaces in molecular graphics: a survey. Comput Graph Forum 36:643–683
45. Yu J, Zhou Y, Tanaka I, Yao M (2010) Roll: a new algorithm for the detection of protein pockets and cavities with a rolling probe sphere. Bioinformatics 26:46–52
46. Trott O, Olson AJ (2010) AutoDock Vina: improving the speed and accuracy of docking with a new scoring function, efficient optimization and multithreading. J Comput Chem 31:455–461
47. Hsin K-Y, Ghosh S, Kitano H (2013) Combining machine learning systems and multiple docking simulation packages to improve docking prediction reliability for network pharmacology. PLoS ONE 8:e83922

48. Yan Y, Zhang D, Zhou P, Li B, Huang S-Y (2017) HDOCK: a web server for protein–protein and protein–DNA/RNA docking based on a hybrid strategy. Nucleic Acids Res 45:W365–W373
49. Huang SY (2015) Exploring the potential of global protein-protein docking: an overview and critical assessment of current programs for automatic ab initio docking. Drug Discov Today 20:969–977
50. Salentin S, Schreiber S, Haupt VJ, Adasme MF, Schroeder M (2015) PLIP: fully automated protein-ligand interaction profiler. Nucleic Acids Res 43:W443–W447
51. Adasme MF, Linnemann KL, Bolz SN, Kaiser F, Salentin S, Haupt J, Schroeder M (2021) PLIP 2021: expanding the scope of the protein-ligand interaction profiler to DNA and RNA. Nucleic Acids Res 49:W530–W534
52. Bowers KJ, Chow E, Xu H, Dror RO, Eastwood MP, Gregersen BA, Klepeis JL, Kolossvary I, Moraes MA, Sacerdoti FD, Salmon JK, Shan Y, Shaw DE (2006) Scalable algorithms for molecular dynamics simulations on commodity clusters. Proceedings of the ACM/IEEE Conference on Supercomputing (SC06), Tampa, Florida, 2006, November 11–17
53. Sastry GM, Adzhigirey M, Day T, Annabhimoju R, Sherman W (2013) Protein and ligand preparation: Parameters, protocols, and influence on virtual screening enrichments. J Comput Aid Mol Des 27:221–234
54. Avbelj F, Moult J, Kitson DH, James MNG, Hagler AT (1990) Molecular dynamics study of the structure and dynamics of a protein molecule in a crystalline ionic environment, Streptomyces griseus protease A. Biochemistry 29:8658–8676
55. Ibragimova GT, Wade RC (1998) Importance of explicit salt ions for protein stability in molecular dynamics simulation. Biophys J 74:2906–2911
56. Hub JS, de Groot BL, Grubmüller H, Groenhof G (2014) Quantifying artifacts in Ewald simulations of inhomogeneous systems with a net charge. J Chem Theory Comput 10:381–390
57. Harder E, Damm W, Maple J, Wu C, Reboul M, Xiang JY, Wang L, Lupyan D, Dahlgren MK, Knight JL, Kaus JW, Cerutti DS, Krilov G, Jorgensen WL, Abel R, Friesner RA (2016) (2016) OPLS3: A force field providing broad coverage of drug-like small molecules and proteins. J Chem Theory Comput 12:281–296
58. Walesa R, Kupka T, Broda MA (2015) Density functional theory (DFT) prediction of structural and spectroscopic parameters of cytosine using harmonic and anharmonic approximations. Struct Chem 26:1083–1093
59. Roos K, Wu C, Damm W, Reboul M, Stevenson JM, Lu C, Dahlgren MK, Mondal S, Chen W, Wang L, Abel R, Friesner RA, Harder ED (2019) J Chem Theory Comput 15:1863–1874
60. Xiong G, Wu Z, Yi J, Fu L, Yang Z, Hsieh C, Yin M, Zeng X, Wu C, Lu A, Chen X, Hou T, Cao D (2021) ADMETlab 2.0: an integrated online platform for accurate and comprehensive predictions of ADMET properties. Nucleic Acids Res 49:W5–W14
61. Bergazin TD, Tielker N, Zhang Y, Mao J, Gunner MR, Francisco K, Ballatore C, Kast SM, Mobley DL (2021) Evaluation of log P, pKa and log D predictions from the SAMPL7 blind challenge. J Comput Aided Mol Des 35:771–802
62. Fischer MJ (2010) Amine coupling through EDC/NHS: a practical approach. Methods Mol Biol 627:55–73
63. Jackson D, Gooya J, Mao S, Kinneer K, Xu L, Camara M, Fazenbaker C, Fleming R, Swamynathan S, Meyer D, Senter PD, Gao C, Wu H, Kinch M, Coats S, Kiener PA, Tice DA (2008) A human antibody-drug conjugate targeting EphA2 inhibits tumor growth in vivo. Cancer Res 68:9367–9374
64. Asyun A, Yagmur K, Yusuf B (2016) Cell proliferation and toxicity assays. Curr Pharm Biotechnol 17:1213–1221
65. Elmore S (2007) Apoptosis: a review of programmed cell death. Toxicol Pathol 35:495–516
66. Vermes I, Haanen C, Steffens-Nakken H, Reutelingsperger C (1995) A novel assay for apoptosis. Flow cytometric detection of phosphatidylserine expression on early apoptotic cells using fluorescein labeled Annexin V. J Immunol Methods 184:39–51
67. Riccardi C, Nicoletti I (2006) Analysis of apoptosis by propidium iodide staining and flow cytometry. Nat Protoc 3:1458–1461
68. Zegzouti H, Zdanovskaia M, Hsiao K (2009) Goueli SA (2009) ADP-Glo: a Bioluminescent and Homogeneous ADP Monitoring Assay for Kinases. Assay Drug Dev Technol 7(6):560–572
69. Thormann M, Klamt A, Hornig M, Almstetter M (2006) COSMOsim: Bioisosteric similarity based on COSMO-RS profiles. J Chem Inf Model 46:1040–1053
70. Atolini O, Olatunji GA (2014) Isolation and evaluation of antiglycation potential of polyalthic acid (furano-terpene) from Daniella Oliveri. J Pharm Anal 5:407–411
71. Mauriello F, Armandi M, Bonelli B, Onida B, Garrone E (2010) H-bonding of furan and its hydrogenated derivatives with isolated hydroxyl of amorphous silica: an IR spectroscopic and thermodynamic study. J Phys Chem C 114:18233–18239
72. Heinzlmeir S, Lohse J, Treiber T, Kudlinzki D, Linhard V, Gande SL, Sreeramulu S, Saxena K, Liu X, Wilhelm M, Schwalbe H, Kuster B, Medard G (2017) Chemoproteomics-Aided Medicinal Chemistry for the Discovery of EPHA2 Inhibitors. ChemMedChem 12:999–1011
73. Himanen JP, Yermekbayevaa L, Janes PW, Walker JR, Xu K, Atapattu L, Rajashankar KR, Mensinga A, Lackmann M, Nikolov DB, Dhe-Paganon S (2010) Architecture of Eph receptor clusters. Proc Natl Acad Sci U S A 107:10860–10865
74. Heinzlmeir S, Kudlinzki D, Sreeramulu S, Klaeger S, Gande SL, Linharess V, Wilhelm M, Qiao H, Helm D, Ruprecht B, Saxena K, Médard G, Schwabe H, Kuster B (2016) Chemical proteomics and structural biology define EPHA2 inhibition by clinical kinase drugs. ACS Chem Biol 11:3400–3411
75. Chrencik JE, Brooun A, Kraus ML, Recht MI, Kolatkar AR, Han GW, Seifert JM, Widmer H, Auer M, Kuhn P (2006) Structural and biophysical characterization of the EphB4 EphrinB2 protein-protein interaction and receptor specificity. J Biol Chem 281:28185–28192
76. Singla N, Goldgur Y, Xu K, Paavilainen S, Nikolov DB, Himanen JP (2010) Crystal structure of the ligand-binding domain of the promiscuous EphA4 receptor reveals two distinct conformations. Biochem Biophys Res Commun 399:555–559
77. Huang S-Y, Zou X (2008) An iterative knowledge-based scoring function for protein-protein recognition. Proteins 72:557–579
78. Huang S-Y, Zou X (2014) A knowledge-based scoring function for protein-RNA interactions derived from a statistical mechanics-based iterative method. Nucleic Acids Res 42:e55
79. Allen WJ, Balius TE, Mukherjee S, Brozell SR, Moustakas DT, Lan PT, Casa DA, Kuntz ID, Rizzo RC (2015) DOCK 6: impact of new features and current docking performance. J Comput Chem 36:1132–1156
80. Huang S-Y (2018) Comprehensive assessment of flexible-ligand docking algorithms: current effectiveness and challenges. Brief Bioinform 19:982–994
81. Gomez-Soler M, Petersen Gehring M, Lechtenberg BC, Zapata-Mercado E, Hristova K, Pasquale EB (2019) Engineering nanomolar peptide ligands that differentially modulate EphA2 receptor signaling. J Biol Chem 294:8791–8805
82. Nowakowski J, Cronin CN, McRee DE, Knute MW, Nelson CG, Pavletich NP, Rogers J, Sang B, Scheinberg DN, Swanson RV, Thompson DA (2002) Structures of the cancer-related aurora-A, FAK, and EphA2 protein kinases from nanovolume crystallography. Structure 10:1659–1667
83. Xie N, Du Q, Li J, Huang R (2015) Exploring strong interactions in proteins with quantum chemistry and examples of their applications in drug design. PLoS ONE 10:e0137113
84. Petty A, Myshkin E, Qin H, Guo H, Miao H, Tochtrop GP, Hsieh J-T, Page P, Liu L, Lindner DJ, Acharya C, Mackerell AD, Ficker E, Song J, Wang B (2012) A small molecule agonist of EphA2 receptor tyrosine kinase inhibits tumor cell migration in vitro and prostate cancer metastasis in vivo. PLoS ONE 7:e42120

85. Guoping N, Li S, Yunfeng P, Duping W (2004) Oleanolic acid inhibits colorectal cancer angiogenesis by blocking the VEGFR2 signaling pathway. Anticancer Agents Med Chem 18:583–590
86. Lipophilicity LCW (2014). In: Stolerman I, Price L (eds) Encylcopeida of Psychopharmacol. Springer, Berlin, pp 1–6
87. Hoa N, Ge L, Kuznetsov Y, McPherson A, Cornforth AN, Pham JTH, Myers M, Ahmed N, Salsman VS, Lamb S, Bowersock JE, Hu Y, Zhou Y, Jadus MR (2010) Glioma cells display complex cell surface topographies that resist the actions of cytolytic effector lymphocytes. J Immunol 185:4793–4803
88. Ko L, Koestner A, Wechsler W (1980) Morphological characterization of nitroscourea-induced glioma cell lines and clones. Acta Neuropathol 51:23–31
89. Bryant MJ, Chuah TL, Luff J, Lavin MF, Walker DG (2008) A novel rat model for glioblastoma multiforme using a bioluminescent F98 cell line. J Clin Neurosci 15:545–551
90. Ahmed S, Mathews AS, Byeon N, Lavasanifar A, Kaur K (2010) Peptide arrays for screening cancer specific peptides. Anal Chem 82:7533–7541
91. Guo G, Yao W, Zhang Q, Bo Y (2013) Oleanolic acid suppresses migration and invasion of malignant glioma cells by inactivating MAPK/ERK signaling pathway. PLoS ONE 8:e72079
92. Ng YP, Chen Y, Hu Y, Ip FCF, Ip NY (2013) Olean-12-eno[2,3-c][1,2,5] oxadiazol-28-oic acid (OEOA) induces G1 cell cycle arrest and differentiation in human leukemia cell lines. PLoS ONE 8:e63580
93. Wei J, Liu M, Liu H, Wang H, Wang F, Zhang Y, Han L, Lin X (2013) Oleanolic acid arrests cell cycle and induces apoptosis via ROS-mediated mitochondrial depolarization and lysosomal membrane permeabilization in human pancreatic cancer cell. J Appl Toxicol 33:756–765
94. Machado C, Schenka A, Vassallo J, Tamashiro W, Goncalves EM, Genari S, Verinaud L (2005) Morphological characterization of a human glioma cell line. Cancer Cell Int 5:13
95. Kumar R, Saneja A, Panda AK (2021) An annexin V-FTIC propidium iodide-based method or detecting apoptosis in a non-small cell lung cancer cell line. Lung Cancer 2279:213–223
96. Saraste A, Pulkki K (2000) Morphologic and biochemical hallmarks of apoptosis. Cardiovascular Res 45:528–537
97. Engeland M, Nieland LJW, Ramaekers FCS, Schutte B, Reutelingsperger CPM (1998) Annexin V-affinity assay: a review on an apoptosis detection system based on phosphatidylserine exposure. Cytometry 31:1–9
98. Reyes-Zurita F, Pachon-Pena G, Lizarraga D, Rufino-Palomares EE, Cascante M, Lupianez JA (2011) The natural triterpene Maslinic acid induces apoptosis in HT29 colon cancer cells by JNK-p53 dependent mechanism. BMC Cancer 11:154
99. Lucio KA, Rocha G, Moncao-Ribeiro LC, Ferandes J, Takiya CM, Gatass CR (2011) Oleanolic acid initiates apoptosis in non-small cell lung cancer cell lines and reduces metastasis of B16F10 melanoma model in vivo. PLoS ONE 6:e28596
100. Singh N, Tiwari S, Srivastava KK, Siddiqi MI (2015) Identification of novel inhibitors of mycobacterium tuberculosis PknG using pharmacophore based virtual screening, docking, molecular dynamics simulation and their biological evaluation. J Chem Inf Model 55:1120–1129
101. Wang Q, Zorn JA, Kuriyan J (2014) Chapter Two. A structural atlas of kinases inhibited by clinically approved drugs. Methods Enzymol 548:23–67
102. Kitagawa D, Gouda M, Kirii Y (2014) Quick Evaluation of kinase inhibitors by surface plasmon resonance using single-site specifically biotinylated kinases. J Biomol Screen 19:453–461